Geological Survey Ireland

Tellus A6 Block: *aempy* Electromagnetic Inversion Report

Geological Survey Ireland is a division of the Department of Communications, Climate Action & Environment.

Geological Survey
Suirbhéireacht Gheolaíochta
Ireland | Éireann

Document Information

Project title: Tellus A6 Block: aempy Electromagnetic Inversion Report Current Document version 1.1 Date 16/07/2020		
Prepared By	**Date**	**Comment**
M. R. Muller	16/07/2020	Responses to review of V1.0 implemented in V1.1

Reviewed By	**Date**	**Comment**
Jim Hodgson	10/06/2020	Review of V1.0

Approved By	**Date**	**Comment**
Jim Hodgson	00/00/0000	

Version History

Ver. No.	**Ver. Date**	**Comment**	**Revised By**
1.0	09/06/2020		M. R. Muller
1.1	16/07/2020	Responses to review of V1.0 implemented in V1.1	M. R. Muller

Table of Contents

1. Introduction

Background to Tellus

Tellus is a national programme to gather geochemical and geophysical data across the island of Ireland. The survey examines the chemical and physical properties of Irish soils, rocks and waters to inform the management of Ireland's environment and natural resources. The project is managed by Geological Survey Ireland (GSI) and is funded by the Department of Communications, Climate Action and Environment (DCCAE).

The Tellus airborne geophysics survey, collecting magnetic, gamma-ray spectrometry and electromagnetic (EM) data, follows on from the initial Tellus Survey of Northern Ireland in 2005-2006, with the first survey in Ireland carried out in 2011. Since then, annual survey blocks have generally progressed southwards through the country. To date, 10 distinct survey blocks have been flown in Ireland (Figure 1.1) with all data processed and made publically available at www.gsi.ie/tellus.

Data from the A5 Survey Block, flown over county Limerick in 2018-2019, were used as the first test case for inversion modelling of Tellus EM data. EM inversion models for the A5 Block were completed and released to the public on 28 February 2020, together with a technical report describing the inversion methodology (GSI, 2020a). Further Tellus EM data blocks are being inverted on an on-going basis. The A6 Block, reported on here, is the third inversion block to be completed (Figure 1.1) and is released simultaneously with the second completed block, Waterford (WFD) (GSI, 2020b).

Background and Rationale for Inversion Modelling

Tellus airborne electromagnetic (EM) data, with the exception of one survey block flown in 2014-2015, are acquired with a four-frequency frequency-domain (FEM) system utilising transmission frequencies at 912, 3,005, 11,962 and 24,510 Hz. Orthogonal in-phase and quadrature components of the EM response at each frequency are recorded and subsequently processed independently of each other, providing eight components of data at each measurement location. The nominal flight speed of 60 m/s and 10 Hz EM

data sampling rate provides measurement locations at approximately 6 m interval along the flight lines.

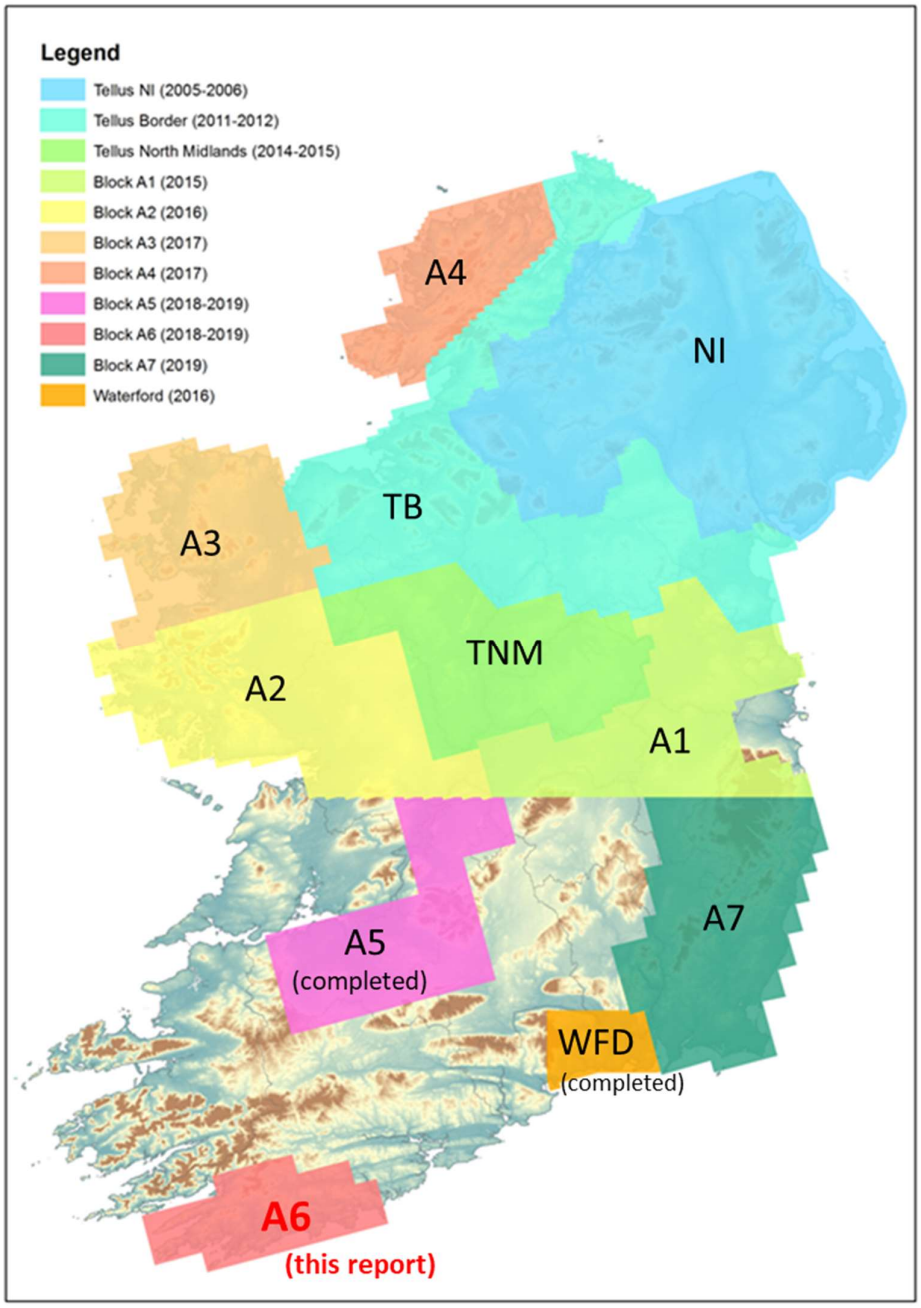

Figure 1.1: Tellus airborne geophysical survey blocks flown to date, shown against topography backdrop. The first Tellus EM inversion models, for Block A5, were completed and released publically on 20 February 2020. A6 Block, the subject of this report, and the third completed EM inversion area, is shown highlighted in red font. The Waterford (WFD) block was the second completed EM inversion area, with models publically released simultaneously with A6 Block.

Geologically more useful subsurface electrical resistivity data can be derived from the eight-component EM response data using a range of different modelling strategies. Prior to the release of the first EM inversion models for the A5 Block, all resistivity products generated and published by the Tellus programme were based on separate and independent modelling of each of the four frequencies, providing independent resistivity data (either as flight-line data or maps) at each frequency (i.e., single frequency modelling). The highest frequency resistivity data, at 24,510 Hz, provide the shallowest, near-surface imaging, while the lowest frequency data, at 912 Hz, provide the deepest subsurface imaging, to depths in the range 40 – 100 m, depending on the subsurface resistivity itself. Greater depths of EM penetration are achieved where the subsurface rock materials are more resistive (i.e., less conductive).

The merged EM resistivity maps (consisting of all contiguous data blocks flown to date), currently published by the Tellus programme for each EM frequency, are derived by Geological Survey Ireland using the *Geosoft HEM* software module. In the *HEM* inversion scheme a single half-space resistivity value is determined through formal inversion that best matches the input in-phase and quadrature data at each measurement location, separately for each of the four EM frequencies.

Published resistivity data for each of the separate, completed survey blocks are also produced by the contractor Sander Geophysics Limited (SGL) using a nomogram (look-up table) approach. In this approach, the resistivity models are generated using the combination of two nomogram-based resistivity algorithms: (i) a pseudo-layer resistivity – for areas of strong signal and (ii) an amplitude-altitude algorithm – for areas of low signal (i.e., high resistivity areas). The nomograms identify a matching half-space resistivity value for in-phase and quadrature data pairs at each measurement location and for each frequency independently.

SGL subsequently use EM skin-depth as a means of estimating approximately the subsurface imaging depth corresponding with each resistivity data point at each frequency. In the skin-depth equation, depth of EM signal penetration (δ, in m) (to $1/e$ of the original signal amplitude) is dependent on the signal frequency (f, in Hz) and the ground resistivity (ρ, in Ω.m):

$$\delta = 503(\rho/f)^{½} \qquad (1)$$

SGL define the depth of imaging (or centroid depth) as $\delta/2$ and, through a process of lateral and vertical interpolation of depth-resistivity pairs derived from each of the four frequencies, produce resistivity-depth data and map slices at 10 m, 30 m, 60 m and 100 m depths. More information on SGL's depth estimation approach may be found, for example, in SGL's A5 Block Technical Report (SGL, 2019), and in Sengpiel (1988) and Sengpiel and Siemon (1998).

While these approximate resistivity-depth products have proven excellent for the mapping of lateral geological variation, they lack the depth resolution and accuracy needed for reliably understanding the geological variation with depth and, for example, for constructing vertical geological cross-sections. GSI has responded to data-users' needs for better depth constraints in the resistivity products offered by Tellus by carrying out formal 1D inversion of the EM response data, modelling all eight EM data components simultaneously at each measurement site. Inversion of the EM data was done using the ***aempy*** suite of software tools, a new open source, *Python* based EM processing and modelling "toolbox" developed by researchers at Dublin Institute for Advanced Studies, funded by a GSI Short Call Research Award (Kiyan and Rath, 2017; Kiyan *et al*., in review). The reasons for electing to use the *aempy* toolbox and for the inversion approach developed around its capacities are discussed further below.

The first EM inversion resistivity models, released in February 2020 by the Tellus Programme, were for the A5 Block (GSI, 2020a). Modelling of all previously flown data blocks is on-going and EM inversion models for these blocks are being released as completed. The A6 Block reported on here is the third data block to undergo EM inversion modelling.

Inversion Approach and Strategy

The need to process and invert large volumes of EM data places a number of requirements on the inversion strategy used and on the inversion codes that support it. The primary requirements are:

i. Automation of the process as far as possible.

ii. Generation of a range of inversion-model quality-control (QC) parameters that can be used collectively for automated, objective rejection of poor model solutions. The recorded EM data are subject to high cultural noise

levels across many parts of Ireland and geological signal strength is strongly attenuated in high-fly zones, both of which impact on the reliability and quality of the EM inversion models.

iii. Relatively fast inversion computational speeds.

Three different commercial and non-commercial codes were tested and assessed by GSI: *EMIGMA* (Petroseikon), *EM1DFM* (University of British Columbia) and *aempy*. All three codes implement similar Tikhonov-type, smooth, regularised 1-D EM inversion schemes and produce similar and comparable output resistivity models. While the *EM1DFM* and *aempy* codes were found to be similar in computation speed, *EMIGMA* is somewhat slower. One of the main advantages of the *aempy* toolbox lies in its *Python* coding, allowing the development of customised scripts for automation and for customised output of inversion models and desired model quality-control parameters. The capacities of the *aempy* toolbox, which include both inversion and pre-inversion processing and filtering tools, are discussed in detail further below.

The inversion workflow is summarised in Figure 1.2 and consists of three main components, implemented as indicated using the facilities of both *aempy* and *Geosoft Oasis Montaj* software: (i) EM and altimeter data pre-processing and filtering, (ii) automated 1-D EM inversion on a line-by-line basis and computation and output of resistivity models and quality-control parameters and (iii) model cleaning (rejection of unreliable model solutions) using quality-control parameters, line-to-line microlevelling and model output. Details of each component of the workflow are discussed in the following sections of the report below, as well as details of the comprehensive tests undertaken to define the optimum control parameters for each workflow component.

The emphasis in the testing and choice of parameters for the inversions and model cleaning process was to identify and use parameters most appropriate for the A6 dataset as a whole – to avoid the inclusion of artefacts and unreliable model solutions in the final delivered model data. It may be the case, therefore, that some resolution and detail is lost in local areas, and which could potentially be recovered using inversion and model cleaning parameters and strategies optimised specifically for those areas. To support Tellus end-users in exploring the possibility of deriving higher resolution EM resistivity models in local areas of interest, the *aempy* software and scripts are made freely available and may be obtained by email enquiry to tellus@gsi.ie.

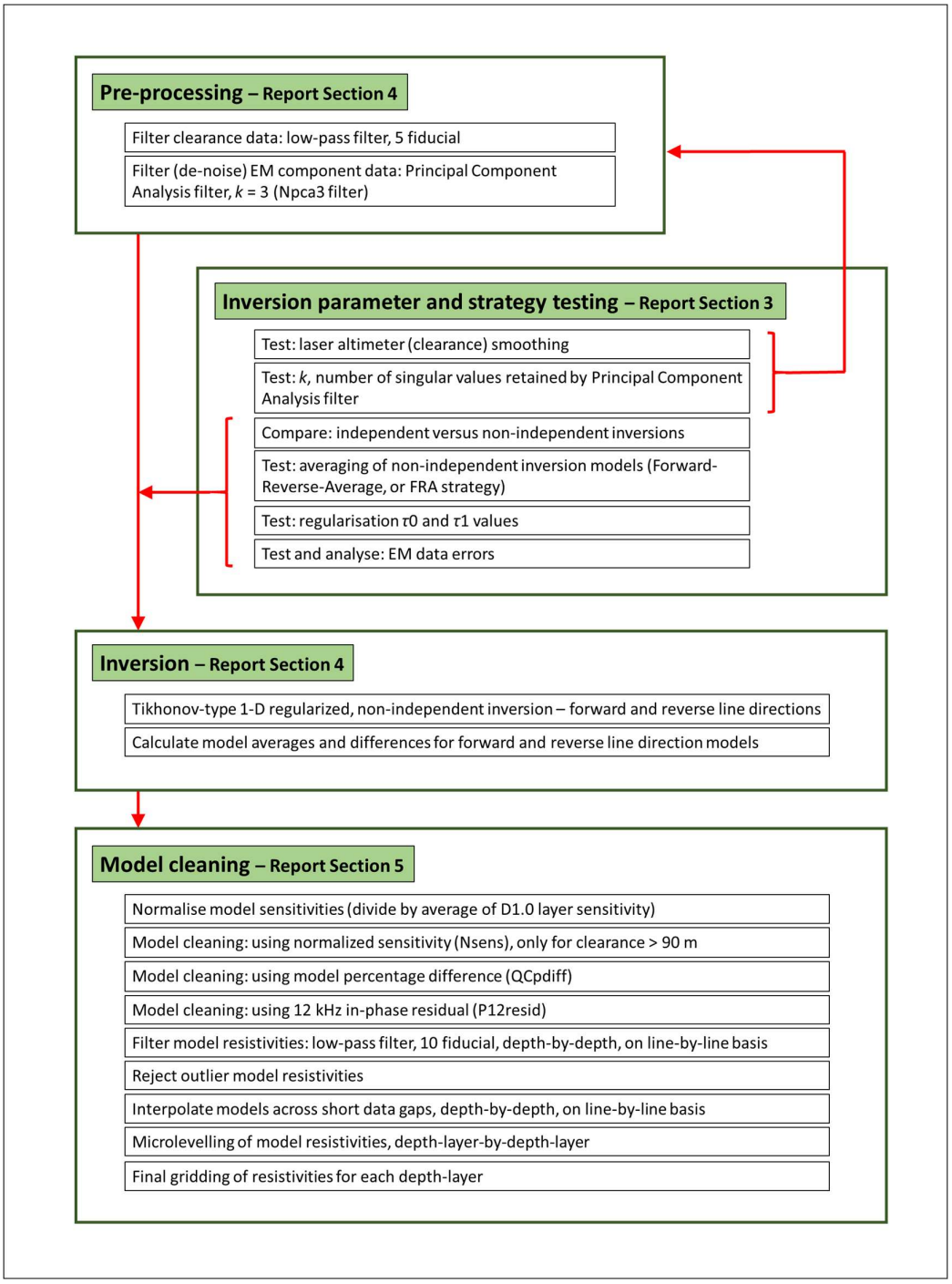

Figure 1.2: Schematic illustration of the EM inversion workflow. Each component of the workflow is discussed further in the text below, in Report Sections referred to in the figure.

Summary of Inversion Products Delivered

EM inversion resistivity models, to a depth of 62.6 m, are made publically available, at www.gsi.ie/telllus, in a number of different data formats.

i. **Ascii, flight-line and site ordered dataset.** Complete, full-resolution dataset **with nominal 6 m spacing between model sites, on flight-lines nominally 200 m apart**. Resistivity data for twenty depth-layers, from 1.0 m to 62.6 m depth, are provided as separate channels (columns) in the dataset. The data are suitable for manipulation to produce either section or map views of the models. Surface topography (DEM) with respect to sea-level is included for each site, allowing models to be plotted beneath a topographic reference in section view.

   File name: [A6_EM_INV_MODELS_OHMM.XYZ].

   File format: *Geosoft* [.XYZ]. Suitable for import into to any software with an ascii import capability.

   Dataset description: Appendix 1.

ii. **Resistivity grids on 50 x 50 m mesh.** Provided separately for twenty depth-layers, from 1.0 m to 62.6 m depth. Inverse Distance Weighted gridding used.

   File formats: *Geosoft* grid [.GRD] and georeferenced tiff [.TIF]

   Dataset description: Appendix 2.

2. *aempy* Toolbox

Overview of Toolbox Utilities

The *aempy* Toolbox (Kiyan and Rath, 2017; Kiyan *et al*., in review) is a flexible package of software providing capacity for the 1-D inversion of frequency- and time-domain airborne EM (AEM) data. The software is written in the *Python* language and calls on several numerical packages in *Python*, namely *numpy*, *scipy* and *matplotlib*. Capacities of the toolbox are implemented in a number of high-level scripts that cover a full work flow from (i) loading and reformatting of raw EM data, (ii) pre-processing of EM responses, (iii) inversion modelling and (iv) visualisation of outputs.

i. Data management tools include reformatting of raw EM data to an internal *aempy* format, data subset selection based on polygons or rectangles, projection of data onto a new profile, and various graphical visualisations of the input data.

ii. EM data pre-processing functions include the masking of non-physical data, interpolation, and Principal Component Analysis (PCA) filtering of data for noise rejection. (In the case of the A6 Block inversion, only PCA filtering was utilised, with no pre-inversion data masking or interpolation applied).

iii. Implementation of several 1-D EM inversion approaches:

- Tikhonov-type regularised inversion. (Used for A6 Block inversion)
- Bayesian MAP (maximum *a posteriori* probability) inversion in parameter and data space. (Not used for A6 Block inversion)
- Full Bayesian Markov Chain Monte Carlo (MCMC) inversion. (Not used for A6 Block inversion).

iv. Various graphical visualisations of: input and filtered EM responses, observed and predicted EM responses (post-inversion), and resistivity model cross-sections.

Tikhonov-type Regularised 1-D Layered Inversion

The computational core of the Tikhonov-type 1-D layered inversion is based on an adapted forward modeller taken from the well-tested ***AirBeo*** open-source (*Fortran 90*) code. This code was originally developed by Australia's CSIRO and the AMIRA consortium (the latest version of which is available from https://sourceforge.net/projects/p223suite). The inversion code in *aempy* is customised for the physical configuration of the current Tellus airborne EM system: the AEM-05 system, which operates at four frequencies (912 Hz, 3,005 Hz, 11,962 Hz, and 24,510 Hz), with vertical, co-planar transmitter and receiver coils (VCP or CpX configuration) mounted at the tips of the aircraft wings with fixed coil separations of 21.35 m for 912 and 3,005 Hz and 21.38 m for 11,962 and 24,510 Hz.

Up to seven geophysical parameters can be included in the 1-D models for inversion: layer thickness, electrical resistivity, relative dielectric constant (although negligible for Tellus EM frequencies), relative magnetic permeability and three Cole-Cole induced polarisation (IP) parameters (chargeability, time constant and frequency constant). The capacity to invert for parameters other than electrical resistivity provides interesting potential when modelling EM data acquired over highly magnetic or polarisable lithologies (e.g., clays and disseminated sulphides). Practically, however, and subject to future testing, it may be difficult to derive reliably such a large number of rock parameters from the four-frequency Tellus data. The A6 Block EM data were inverted for a single parameter only, resistivity, using fixed layer thicknesses and depths for all sites (defined in Table 4.2, Section 4). The single-parameter, fixed-layer inversions should, in principle, provide the best possible resolution in estimating resistivity values.

On the data input side of the inversion, any of the individual eight EM data components can be flagged as active or inactive for the inversion (all eight components were flagged active for the A6 Block inversion) and data errors for the eight components can be individually specified. EM measurement sites can be excluded from the inversion using flight clearance and power-line monitor thresholds (neither threshold was applied to exclude data for the A6 Block inversion).

The theoretical and numerical basis for the Tikhonov-type inversion scheme implemented in *aempy* is outlined in detail Kiyan and Rath (2017) and Kiyan *et al*. (in

review). From a practical user's perspective, there are three parameters requiring definition that control the inversion and the characteristics of the output models: the data errors, and the two regularisation parameters, $\tau 0$ and $\tau 1$. The parameter $\tau 0$ controls the freedom of the inversion model to diverge from the defined starting (*a priori*) model, with larger $\tau 0$ values providing less freedom. The parameter $\tau 1$ controls the smoothness of the model (in a 1-D vertical sense), with larger $\tau 1$ values producing smoother models. Assignment of a data error to each of the EM data components controls the weighting placed on those components in the inversion. Lower errors provide a stronger weighting. Data errors therefore have the practical effect of focussing the inversion on different regions of the subsurface: for example, lower errors assigned to higher frequency data will tend to weight the inversion towards resolving shallower resistivity structure, and *vice versa* for lower errors assigned to lower frequency data and deeper structure. Given the importance of these three parameters in controlling the inversion outputs, it is beneficial to carry out tests on the inversion dataset, to identify appropriate values for them and to understand how their variation affects the shape and quality of fit of the output models (such tests were carried out for the A6 Block data, as reported in Section 3).

A valuable, post-inversion output provided by the *aempy* code is the model sensitivity matrix (essentially the inversion Jacobian matrix). It describes the sensitivity of the EM responses to changes in the model resistivity, separately for each layer at depth in the model. Numerically, sensitivity, S, is defined as the derivative of the EM response, $g(m)$, with respect to the model parameter, m (resistivity):

$$S = \partial g(m)/\partial m \qquad (2)$$

where the net sensitivity is provided by the sum of the sensitivities of all eight data responses (components). Where a large change in model resistivity (for a particular depth layer) produces a small change in the predicted EM response, that part of the model might be regarded as poorly constrained, as the EM data are insensitive to it. As the Jacobian matrix in the inversion is weighted by the data errors, higher data errors lead to lower model sensitivities. Sensitivities are intimately connected to the specifics of the EM data acquisition system and the inversion parameterisation: e.g., the frequencies used and the coil geometry, the flight clearance, the data errors assigned, and the thickness of the model layers (thinner layers have lower sensitivities). It is

therefore very difficult to assign a universal sensitivity threshold above which a model solution might be regarded as reliable. Nevertheless, sensitivity can be used as a practical means of identifying and rejecting poorly constrained parts of the inversion models (and in the case of the A6 Block has been used both to identify a maximum depth of reliable investigation and to reject poor model solutions in high-fly areas, as discussed in Sections 4 and 5).

Principal Component Analysis Filter

Electromagnetic noise levels are relatively high across many parts of Ireland, originating from multiple cultural noise sources such as power-lines, gas pipelines, towns, industrial centres, farms and dwellings, and have a detrimental effect on the EM response data, particularly at the low 0.9 and 3 kHz transmission frequencies. One particularly useful utility within the *aempy* toolbox is a noise rejection filter based on a Principal Component Analysis (PCA) and decomposition of the EM response data. In this approach, the EM dataset is reconstructed using the strongest and most coherent principal components only, with the weaker principal components (noise) rejected. Previous applications of the approach to airborne EM data (Reninger *et al*., 2011; Minsley *et al*., 2012) have illustrated good success in reducing noise contamination and in imposing regularity (consistency) on the data.

In *aempy*, the PCA is based on the singular value decomposition (SVD) (Lanczos, 1961; Golub and van Loan, 1996) of the data observation matrix, D, which has n_{data} rows and n_{site} columns. After removing the average of the rows, matrix D can be decomposed into an orthonormal set of basis functions using the SVD:

$$D = USV^T \qquad (3)$$

where U and V are unitary matrices, and S is diagonal and contains the singular values in decreasing sequence. By choosing the k largest values in S and truncating the matrices correspondingly, an approximate matrix D' is obtained, which contains only the coherent components of D. Matrix D' is thus an output filtered (de-noised) version of the input data matrix D.

In the context of Tellus EM data, the number of data rows in matrix D is equal to eight (in-phase and quadrature components for 4 frequencies) and as the filter is applied on a

line-by-line basis in *aempy*, the number of site columns in matrix *D* is equal to the number of sites on the flight line. Choice of an optimal value for *k*, the number of singular values to be retained in the reconstructed (filtered) data, is considered in Section 3 below.

3. Inversion Parameter Testing

Two A6 Block data subsets (Figures 3.1 and 3.2) were used to test several aspects of the inversion workflow and to test the parameter settings that control the *aempy* Tikhonov-type 1-D inversion:

i. **Test Dataset A**: Five approximately 15.4 km-long lines: L6307 (west) to L6311 (east), with 2,280, 2,479, 2,344, 2,674 and 2,356 sites on each line respectively.

ii. **Test Dataset B**: An approximately 4.2 km-long section on line L6310, with 734 sites on the line.

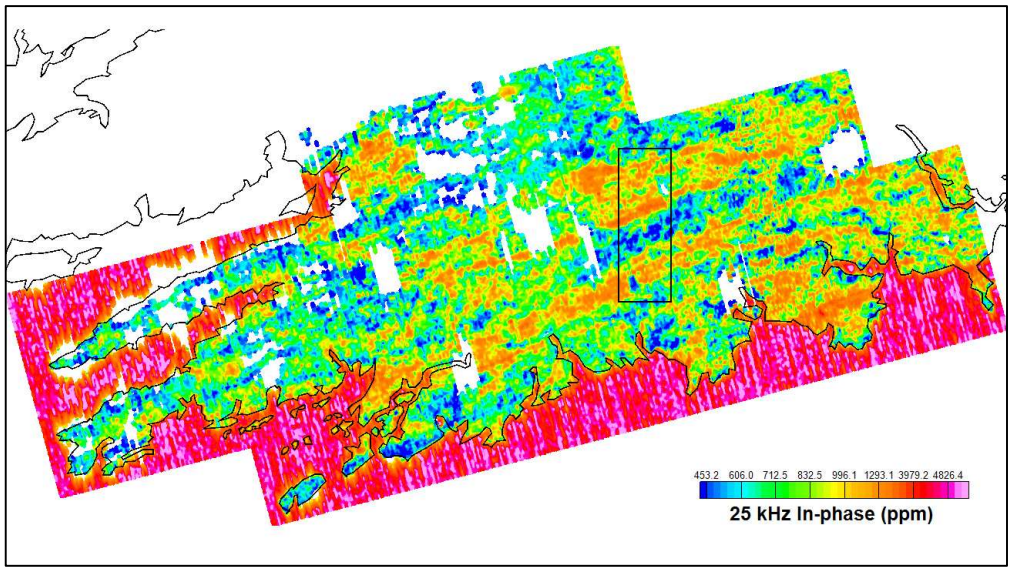

Figure 3.1: Data area (black polygon) used for inversion parameter tests, shown against 25 kHz in-phase data grid. The polygon contains 5 test flight lines from L6307 (west) to L6311 (east). Long axis of polygon is ~14.9 km in length. Detail shown in Figure 3.2. The 25 kHz in-phase data are blanked where flight clearance > 120 m (for display only, not for inversion). Irish coastline (black line) shown.

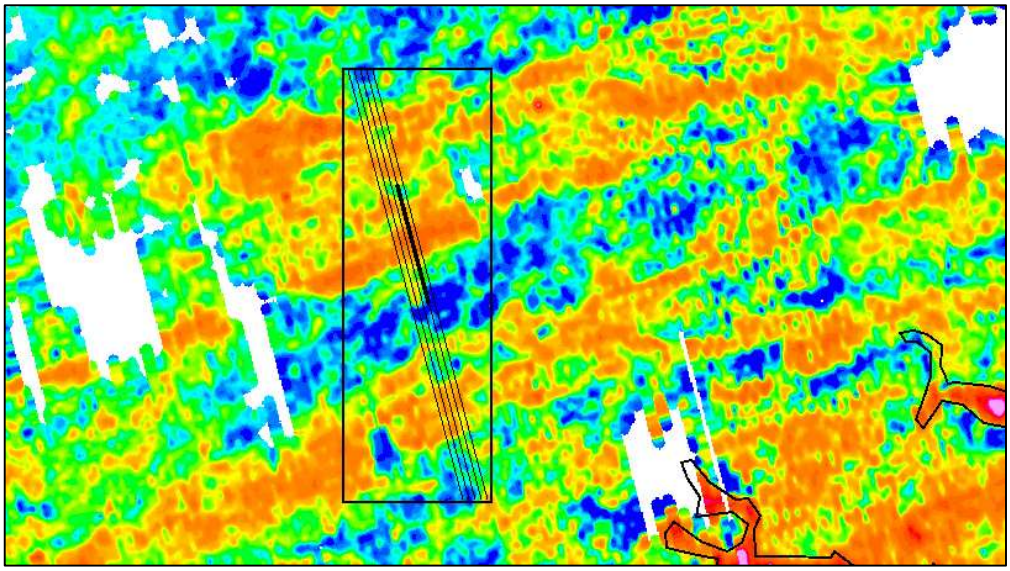

Figure 3.2: Detail of data subsets used for parameter testing, shown against 25 kHz in-phase data grid. Black polygon shows test area containing two data subsets (A and B) used variously for different tests: (A) thin lines show five ~15.4 km-long flight lines, from L6307 (west) to L6311 (east) and (B) thicker black line shows ~4.2 km long test portion of L6310. The 25 kHz in-phase data are blanked where flight clearance > 120 m (for display only, not for inversion). Irish coastline, where present, shown (black line).

A range of inversion tests and runs were carried out (Table 3.1.) to examine different aspects of the inversion workflow, the results of which are expanded on in more detail in the sections below.

i. Laser altimeter (clearance) smoothing.

ii. Application of Principal Component Analysis noise-rejection filter.

iii. Fully independent 1-D inversion of each site versus non-independent 1-D inversion (i.e., the latter using the previous site's model as the *a priori* (starting) model for the current site).

iv. Single line direction, non-independent inversion models versus forward and reverse line direction model averaging.

v. Regularisation parameters for Tikhonov-type inversion: $\tau 0$ (closeness to starting model) and $\tau 1$ (model smoothness).

vi. EM data component errors (for in-phase and quadrature for each frequency independently). Assessed for A5 Block and not for A6 (see GSI, 2020a).

The effect of different EM data component errors was comprehensively assessed previously for the inversion of Block A5 and has not been re-assessed for the A6 Block inversion, as noted above. Further details on the A5 Block tests and assessments may be found in GSI (2020a). Note that the parameters for Tests 1 – 6 and Tests 7 – 12 are identical, except for a 5-fiducial low-pass filter being applied to the laser altimeter clearance data in the case of the former group, while a 20-fiducial low-pass filter was applied in the case of the latter group.

Laser Altimeter (Clearance) Smoothing

Aircraft clearance data (aircraft height above ground level) are a required input into the *aempy* inversion code – as the amplitudes of EM responses are strongly dependent on EM sensor height above ground level. In the case of the contractor-delivered EM dataset, clearance data are derived from the aircraft's laser altimeter and are subject to noise spikes that are largely the result of unreliable laser reflectance when flying over areas of thick, tall or variable vegetation cover.

Tests carried out on data from the A5 Block (GSI, 2020a) indicate that raw (unfiltered) laser altimeter data, when used as input, produce spurious "spikes" in the 1-D inversion models at locations corresponding with laser altimeter spikes. Confirmation that laser altimeter spikes are not a reflection of real, sudden changes in flight altitude is provided by the absence of changes in the EM responses coincident with the altimeter spikes. Clearance spikes can also translate into spurious spikes in the model topographic surface - as surface topography is derived from the clearance data (by subtraction of clearance data from the aircraft GPS Z data – see Equation 4 below). In the case of the A5 Block, a 20-fiducial (~120 m wavelength) low-pass filter was found to provide optimal results in de-spiking the clearance data. However, the clearance data in the A6 Block reflect significant topographic variation on a much shorter length scale than 120 m, associated with the very rugged topography of southern Co. Cork and in particular the peninsulas and islands of the south-western coastline. A more moderate 5-fiducial (~30 m wavelength) low-pass filter, applied to the clearance data, was therefore tested in a number of inversion runs (Tests 1 – 6) against the 20-fiducial filter (Test 7 – 12).

Table 3.1: Summary of inversion runs to test aspects of the inversion strategy and to identify optimum inversion regularisation parameters. The final A6 delivery dataset used for the tests is [GSI___18.IRL_DLV2159_FEM.xyz], the same as used for the production inversion. All tests were run with 35-layer 1-D models, with a shallowest layer thickness of 2 m increasing logarithmically (log_{10}) with depth to a final layer thickness of 10 m. Test datasets A and B are described in the text above. The FRA strategy (short for "forward-reverse-average" strategy) refers to running non-independent inversions in both line directions, and deriving an average model from the two model solutions at each site, as well as computing the differences between the two models for quality control purposes.

Test no.	Test dataset	Low-pass filter applied to clearance data	PCA (*k*=3) filter applied to EM data	Indep. Models	Strategy	Data errors (ppm)	τ0	τ1	No. of sites	Comment
1	A	5-fiducial	No	No	FRA	All 60.0	0.01	6.0	12,133	Inversion test without Npca3 filter applied.
2	A	5-fiducial	Yes	No	FRA	All 60.0	0.01	6.0	12,133	Inversion test with Npca3 filter applied.
3	B	5-fiducial	No	No	Fwd. only	All 60.0	0.01	1 - 100 (40 tests)	734	Tau1 test, with Tau0=0.01. Npca3 filter not applied.
4	B	5-fiducial	Yes	No	Fwd. only	All 60.0	0.01	1 - 100 (40 tests)	734	Tau1 test, with Tau0=0.01. Npca3 filter applied.
5	B	5-fiducial	Yes	Yes	Indep. models	All 60.0	0.01	1 - 100 (40 tests)	734	Tau1 test, with Tau0=0.01. Npca3 filter applied. Independent inversions.
6	B	5-fiducial	Yes	No	Fwd. only	All 60.0	0.001 - 1 (60 tests)	2.89427	734	Tau0 test, with Tau1=2.89427, Npca3 filter applied.
7	A	20-fiducial	No	No	FRA	All 60.0	0.01	6.0	12,133	Inversion test without Npca3 filter applied.
8	A	20-fiducial	Yes	No	FRA	All 60.0	0.01	6.0	12,133	Inversion test with Npca3 filter applied.

9	B	20-fiducial	No	No	Fwd only	All 60.0	0.01	1 - 100 (40 tests)	734	Tau1 test, with Tau0=0.01. Npca3 filter not applied.
10	B	20-fiducial	Yes	No	Fwd only	All 60.0	0.01	1 - 100 (40 tests)	734	Tau1 test, with Tau0=0.01. Npca3 filter applied.
11	B	20-fiducial	Yes	Yes	Indep. models	All 60.0	0.01	1 - 100 (40 tests)	734	Tau1 test, with Tau0=0.01. Npca3 filter applied. Independent inversions.
12	B	20-fiducial	Yes	No	Fwd only	All 60.0	0.001 - 1 (60 tests)	2.89427	734	Tau0 test, with Tau1=2.89427, Npca3 filter applied.

It is noted that surface topography referenced to sea-level, *DEM*, is derived from the clearance and aircraft GPS Z coordinate (*MSLHGT*) data:

$$DEM = MSLHGT - CLEARANCE \quad (4)$$

DEM data derived using Equation 4, for each model location, are included in the final ascii model data files delivered by the Tellus programme.

Figures 3.3 and 3.4 compare clearance data filtered with 5-fiducial and 20-fiducial low-pass filters on two ~4 km-long profiles, together with observed in-phase and quadrature EM responses. As observed for the A5 Block tests, the features and wavelengths observed in the 20-fiducial filtered clearance data are commensurate with those seen in the recorded EM responses. There is little evidence in the observed responses of the shorter wavelength variations seen in the 5-fiducial filtered clearance data. There is evidence, however, of degradation of sharper features in the topographic profile produced by the 20-fiducial filter, particularly on the rugged coastline (Figure 3.3).

A comparison of inversion model results, for line L6310 (Dataset B), derived using 5-fiducial and 20-fiducial filtered clearance data reveals no appreciable difference between the two (Figure 3.5), with identical average RMS errors of 1.064 recorded for both models. The comparison takes inversion results from Test 4 (5-fiducial LP filter) and Test 10 (20-fiducial filter) (Table 3.1), with identical inversion parameters used, except for the filter applied to the clearance data.

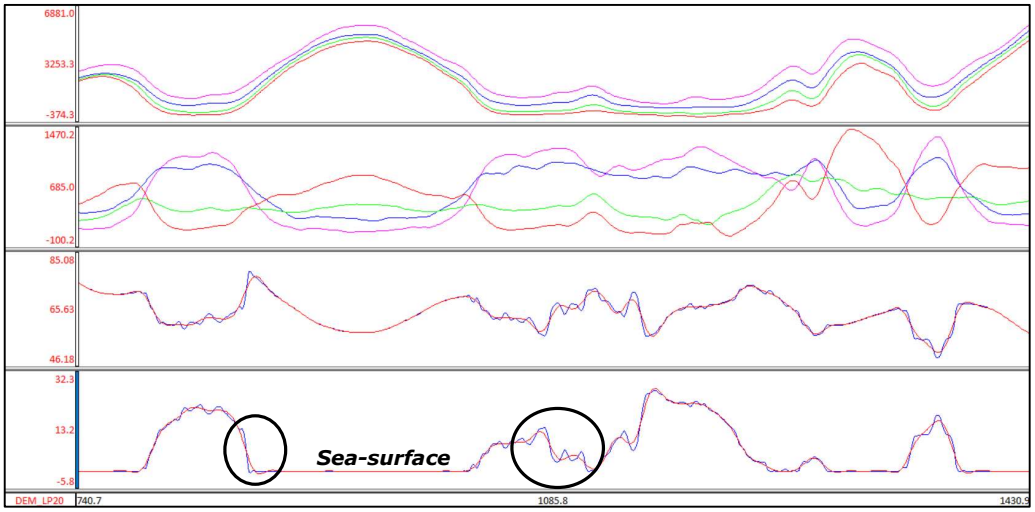

Figure 3.3: Line L6142 profile display (4.4 km long section) showing: (top panel) in-phase responses at 0.9, 3, 12 and 25 kHz (red, green, blue and purple respectively); (upper middle panel) quadrature responses at 0.9, 3, 12 and 25 kHz (red, green, blue and purple respectively); (lower middle panel) 5-fiducial low-pass filtered clearance data (blue) and 20-fiducial low-pass filtered clearance data (red); (bottom panel) DEM referenced to sea-level calculated from 5-fiducial low-pass filtered clearance data (blue) and 20-fiducial low-pass filtered clearance data (red). Circles in bottom panel highlight areas of loss of sharpness in the topographic profile derived using the 20-fiducial clearance data. North is to the right-hand side of the profiles.

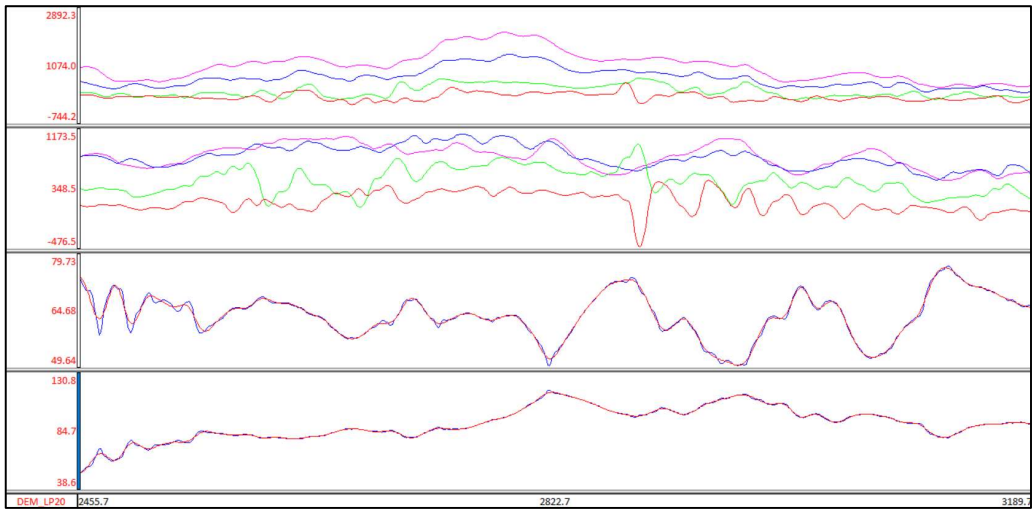

Figure 3.4: Line L6310 profile display (4.2 km long section, Test Dataset B) showing: (top panel) in-phase responses at 0.9, 3, 12 and 25 kHz (red, green, blue and purple respectively); (upper middle panel) quadrature responses at 0.9, 3, 12 and 25 kHz (red, green, blue and purple respectively); (lower middle panel) 5-fiducial low-pass filtered clearance data (blue) and 20-fiducial low-pass filtered clearance data (red); (bottom panel) DEM referenced to sea-level calculated from 5-fiducial low-pass filtered clearance data (blue) and 20-fiducial low-pass filtered clearance data (red). South is to the right-hand side of the profiles.

Given the absence of differences between the inversion models produced with the 5-fiducial and 20-fiducial filters and considering the potential value of a higher fidelity topographic profile in local-scale studies using the output inversion models, it was decided to **use the 5-fiducial low-pass filter, applied to the clearance data, prior to production inversion of the A6 Block.**

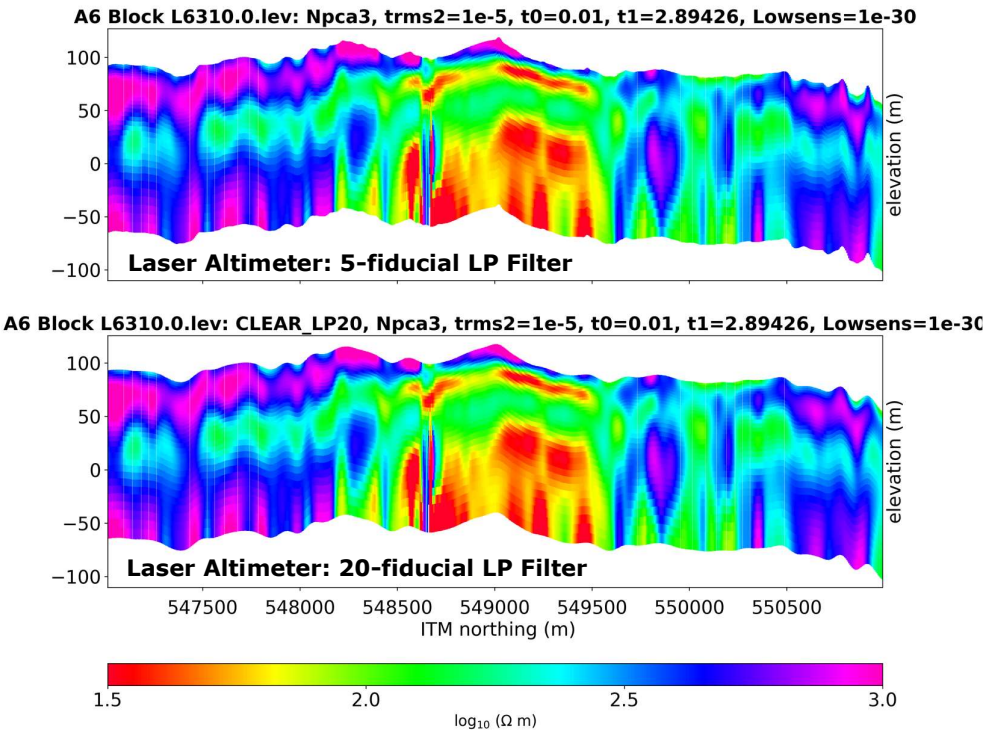

Figure 3.5: Line L6310 (Test Dataset B): Comparison between EM inversion resistivity models computed using (top) 5-fiducial low-pass filtered laser altimeter data and (bottom) 20-fiducial low-pass filtered laser altimeter data as input. The 2-D sections shown are the result of plotting the 1-D resistivity models computed at each site along the profile. Colour scale used has conductive bodies shown in red and resistive bodies in blues/purples. North is to the right-hand side of the profiles.

Principal Component Analysis Noise-Rejection Filter

The Principal Component Analysis filter, described in Section 2 above, is applied prior to EM inversion with the objective of reducing noise and imposing regularity and consistency on the EM response data. In decomposing the EM data into amplitude-ordered singular values (principal components), the critical decision in reconstructing, and thereby effectively filtering, the data lies in the selection of the cut-off between significant, coherent principal components (which will be retained) and incoherent, insignificant principal components (noise, which will be rejected) – i.e., choosing the value for *k*, where the largest *k* values in the singular value matrix *S* are retained (see Section 2).

An examination of the EM data recorded at multiple flight heights over the Tellus Bundoran Test Line (Kiyan *et al*., in review) indicates that most of the coherent data are

present in the first two principal components (or singular values) (Figure 3.6). In the upper panel of Figure 3.6, it is apparent that all singular value amplitudes are low for flight heights equal to and greater than 120 m; that significant amplitudes are found in singular values 1 and 2 for flight heights of 90 m and lower; and that significant amplitudes are found in singular values 1, 2 and 3 for flight heights of 80 m and lower.

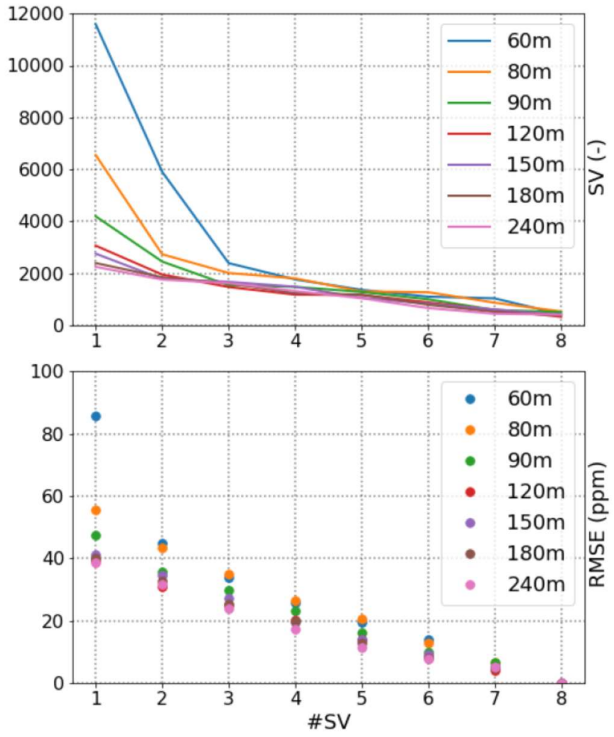

Figure 3.6: Summary of Singular Value Decomposition (SVD) analysis results for Tellus Bundoran Test Line data for seven flight altitudes, flown in 2015. (Upper panel) shows singular value amplitude (SV) for each singular value (#SV). (Lower panel) shows the root-mean-square error (RMSE) between the observed data and the reconstructed data versus singular value number (#SV). In the lower panel, for example, the data plotted at #SV = 3 correspond with the RMS error between the recorded data and the reconstructed data using singular values 1, 2 and 3 (i.e., using k = 3). From Kiyan et al. (in review).

The effect of applying the PCA filter to the EM data can be assessed by examining the differences between the input and filtered data. In the lower panel of Figure 3.6, a comparison is made using the root-mean-square error (or difference) between the input and filtered data, as a function of the number of singular values (principal components) retained in the data reconstruction. In this lower panel, for example, the data plotted at #SV = 3 correspond with the RMS error between the recorded (input) data and the data

reconstructed using singular values 1, 2 and 3 only. Retaining all eight singular values (#SV = 8) reconstructs the input data exactly, returning an RMS error of zero. Whether the filtered data satisfactorily capture the coherent signal in the recorded data depends on the data errors estimated for the recorded data themselves. Given that the average data error for all eight EM data components is unlikely to be less than 40 ppm (as discussed in more detail in the "EM Component Data Errors" section below), it is apparent in Figure 3.6 (lower panel) that only singular values 1 and 2 are required to reconstruct the data to within the data observational error and that higher singular values are essentially contributing noise.

In taking a conservative approach in applying the PCA filter to the data of A6 Block, principal components 1, 2 and 3 have been used in the data reconstruction (i.e., using k = 3), reducing the possibility of rejecting some coherent geological signal and allowing for lower than average noise levels in some of the eight EM data components. Figure 3.7 compares the recorded (input) data and PCA filtered data for k = 3 for Line L6310 from Test Dataset A (this filter, for brevity and convenience, is referred to as the "Npca3" filter in the text). The most obvious impacts of the Npca3 filter observed in the L6310 data are the removal of several high-amplitude (noise) spikes in the low frequency, in-phase 0.9 and 3 kHz data components and a general smoothing of the data for all eight data components.

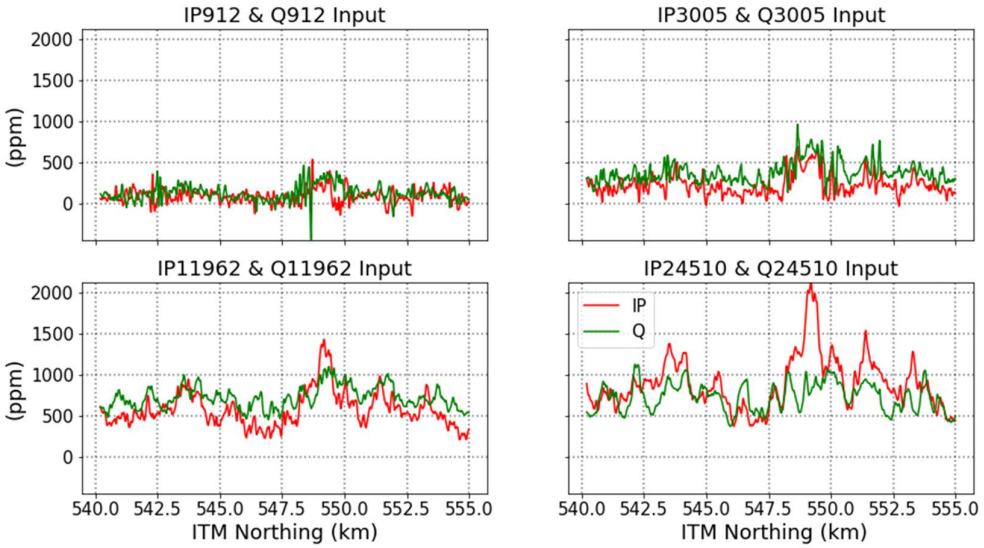

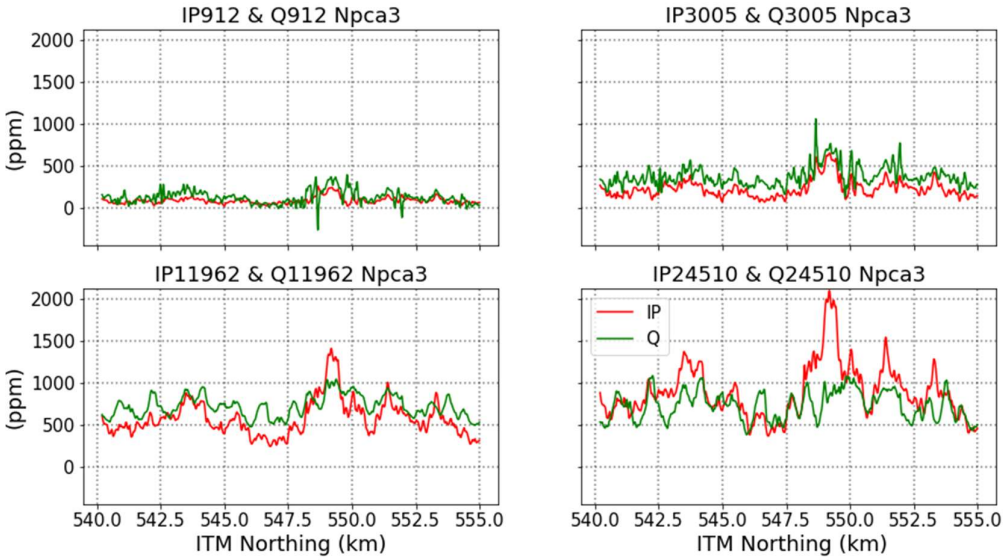

Figure 3.7: Line L6310 (Test Dataset A): (Upper four panels): recorded (input) data for in-phase (IP) and quadrature (Q) components for 912, 3,005, 11,962 and 24,510 Hz frequencies. (Lower four panels): PCA filtered data (k = 3, Npca3) for in-phase (IP) and quadrature (Q) components for 912, 3,005, 11,962 and 24,510 Hz frequencies. North is to the right-hand side of the profiles.

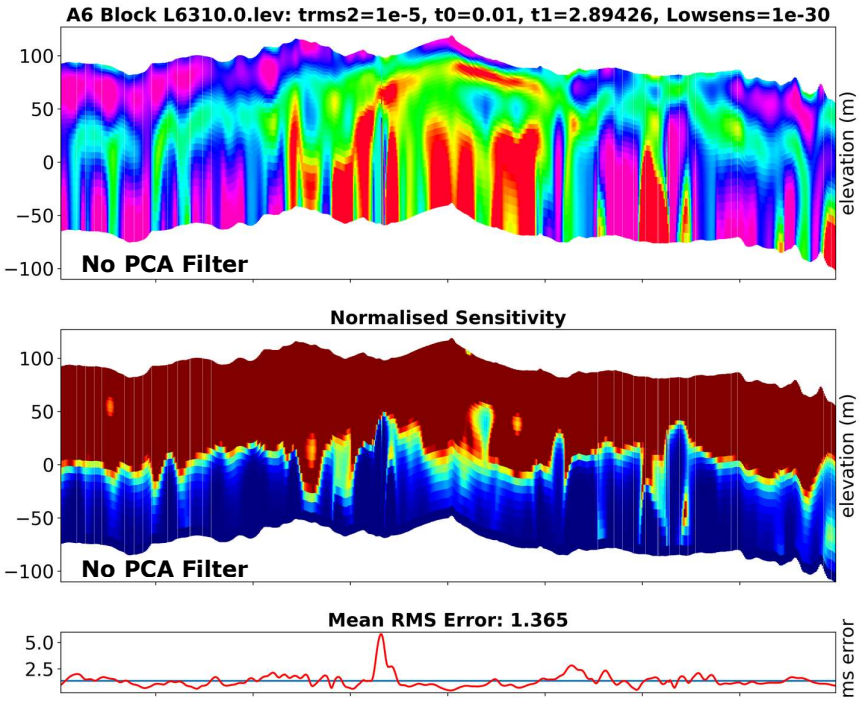

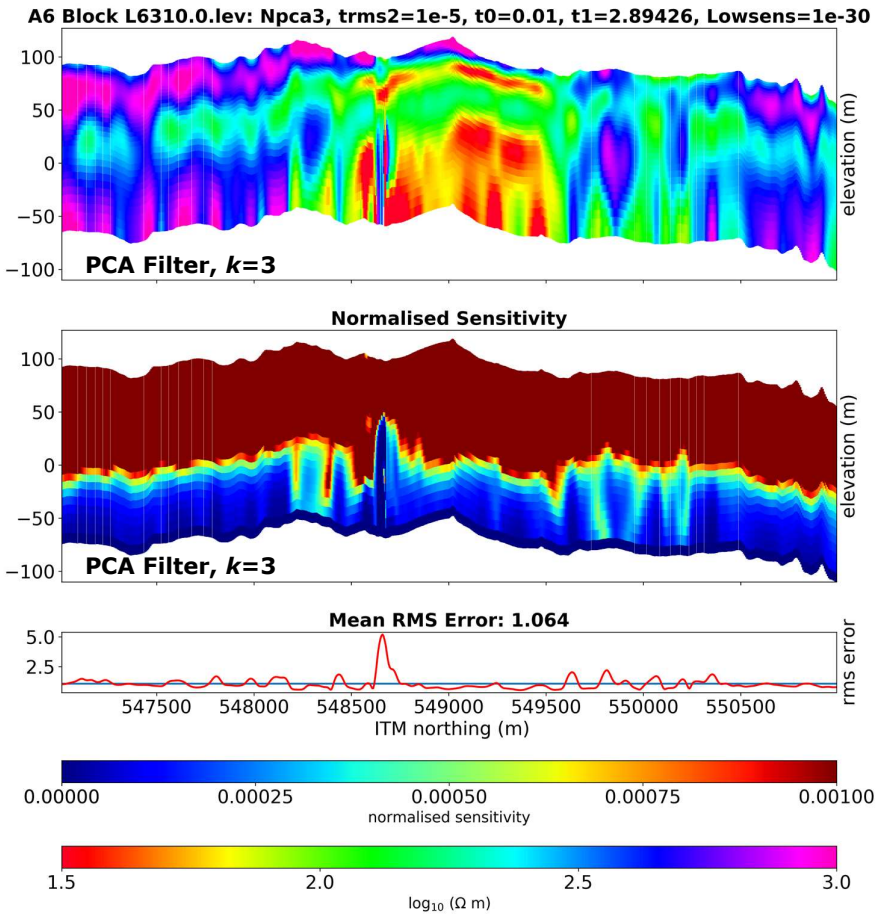

Figure 3.8: Line L6310 (Test Dataset B): Comparison between EM inversion resistivity models computed (top three panels) without PCA filter and (bottom three panels) with PCA filter, retaining first three principal components. Inversion regularisation parameters used in both cases are τ0 = 0.01 and τ1 = 2.894. Normalised model sensitivity sections and profiles of RMS error at each site are shown below the model sections. The sensitivity normalisation factor used is the maximum sensitivity for the profile, determined separately for each profile. Horizontal blue line shows the mean RMS error for the profile. In both inversions, flight clearance data are low-pass filtered (5-fiducial). Resistivity colour scale used has conductive bodies shown in red and resistive bodies in blues/purples. North is to the right-hand side of the profiles.

Figure 3.8 compares *aempy* inversion model results for L6310 (Test Dataset B) derived using unfiltered EM data (inversion Test 3, Table 3.1) and the Npca3 filtered data (inversion Test 4). Except for the application of the Npca3 filter, the two test inversions are identical in their parameters ($\tau 0$ = 0.01 and $\tau 1$ = 2.894). The unfiltered and Npca3 filtered data models return mean profile RMS errors (misfits) between the observed and predicted responses of 1.365 and 1.064 respectively. With the exception of a short section on both models at around ITM Y coordinate 548,700 m, where RMS errors are

higher with a maximum in excess of 5.0, site RMS errors are generally low across the length of profiles, oscillating around the average error. Note that the RMS errors reported by *aempy* are normalised by the data errors – specified as 60.0 ppm for all data components in the case of these two tests – and an RMS error = 1 would indicate a fitting of the observed data to within data error.

In comparing the two models of Figure 3.8, the Npca3 filtered result shows generally improved resistivity model continuity and coherence, as well as improved stability in model sensitivity. The lateral continuity of the conductor at around 25 m depth below surface in the central portion of the profile is visibly improved in the Npca3 inversion. There is no evidence of loss of geological detail with respect to the unfiltered result, indicating that the Npca3 filter has not removed coherent geological signal from the EM data. The absence of significant differences in the main features recovered in the two models suggests that the reduction in the average RMS error for the Npca3 model is primarily due to the removal of noise in the data (i.e., noise that can't be fit by the inversion modelling in the unfiltered data).

On the basis of the above results, the Npca3 filter (PCA filter, with *k* = 3) was therefore applied to EM response data prior to production inversion of the A6 Block.

Independent versus Non-independent Inversion

The *aempy* Tikhonov-type inversion code provides two options for the *a priori* (starting) model used at each EM measurement site (keeping in mind that the 1-D inversions are run on a line-by-line basis):

i. a half-space with a user defined resistivity value, referred to here as ***"independent"*** inversion, and

ii. the previous site's resistivity model (with the starting model for the first site on the line being a half-space with a user defined resistivity value), referred to here as ***"non-independent"*** inversion.

Similar to other geophysical methods, EM modelling is subject to the concept of equivalence – in which different possible model solutions can satisfy equally well the observed EM response data, to within data error. The EM method is particularly sensitive to conductive subsurface bodies, specifically to their conductance (the

conductivity-thickness product), and is therefore particularly subject to equivalence in the modelling of conductors (i.e., a thinner, more conductive body producing an equivalent EM response to a thicker, less conductive body).

In running independent inversions at each site, there is no restriction placed on the possibility of adjacent sites converging on different, but equivalent, model solutions, potentially leading to discontinuous or blocky resistivity model sections along flight lines. The use of the previous site's model as the starting model, as done in the non-independent inversions, attempts to direct the inversion towards convergence on a model that does not deviate dramatically from the previous site's model, unless required to do so by the EM data. Choice of the inversion regularisation parameter $\tau 0$, which controls the freedom of divergence from the starting model, provides a means of controlling how rapidly site-to-site inversions can respond to lateral changes in geology when using non-independent modelling (see the "Inversion Regularisation Parameters" section below for further discussion).

Test inversions carried out confirm a tendency for independent inversions to produce less continuous model sections along flight lines - with a certain "blockiness" apparent as model solutions transition from one set of similar models to a different (but equivalent) set of models along the line – as illustrated in the example of L6310 (from Test Dataset B) in Figure 3.9. The same discontinuity is also apparent in the normalised sensitivity section and RMS error profile for the independent inversion. The independent inversion result in Figure 3.9 is taken from inversion Test 5 (Table 3.1), where a 100 Ω.m starting model was used, delivering a mean RMS error for the line of 1.256, and the non-independent inversion result from Test 4, where a 100 Ω.m starting model was used for the first site on the line, delivering a mean RMS error of 1.064. The same inversion regularisation parameters were used in both cases ($\tau 0 = 0.01$ and $\tau 1 = 2.894$).

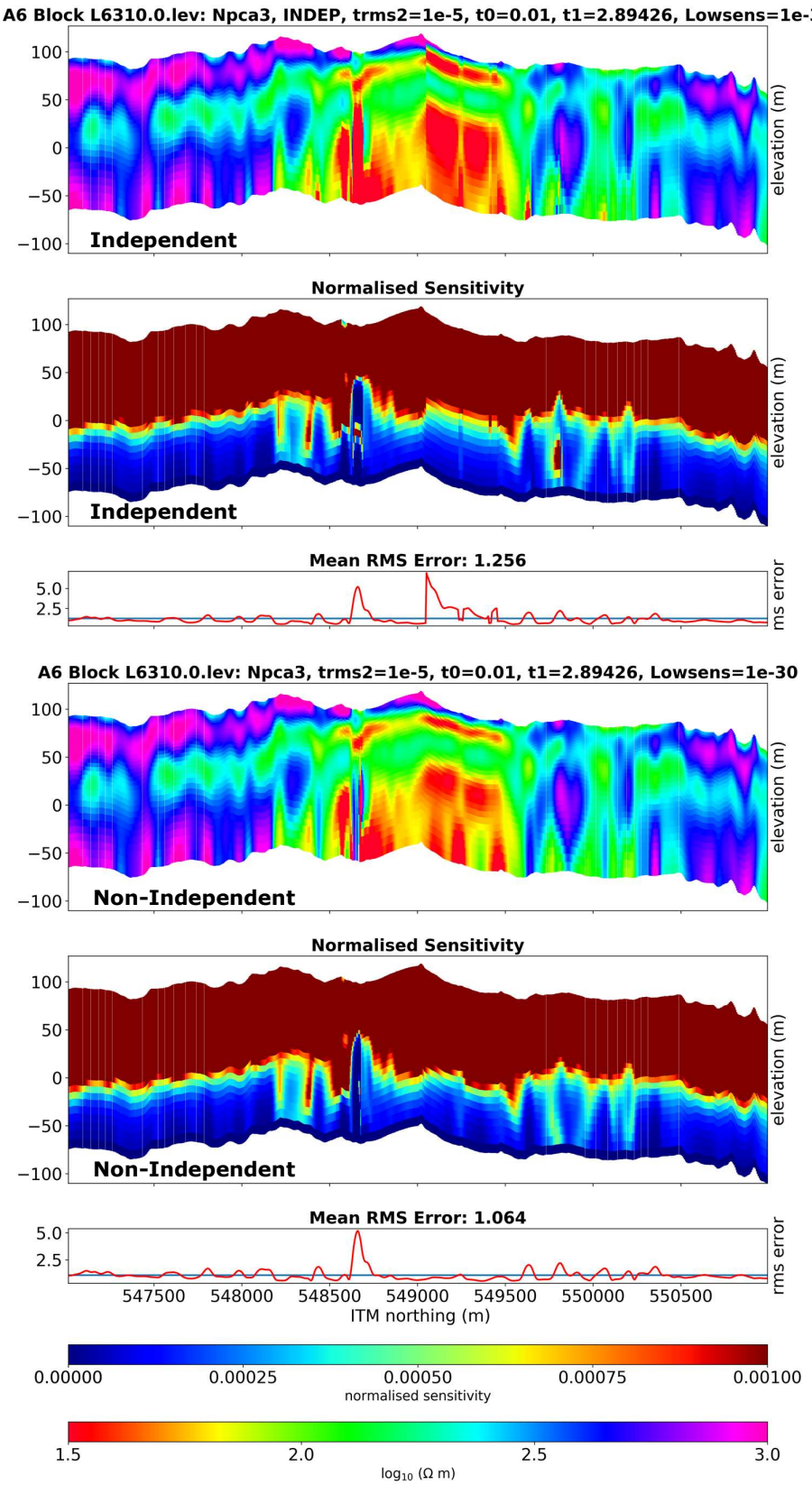
A6 Block L6310.0.lev: Npca3, INDEP, trms2=1e-5, t0=0.01, t1=2.89426, Lowsens=1e-30
Independent
elevation (m)
Normalised Sensitivity
Independent
elevation (m)
Mean RMS Error: 1.256
ms error
A6 Block L6310.0.lev: Npca3, trms2=1e-5, t0=0.01, t1=2.89426, Lowsens=1e-30
Non-Independent
elevation (m)
Normalised Sensitivity
Non-Independent
elevation (m)
Mean RMS Error: 1.064
rms error
547500 548000 548500 549000 549500 550000 550500
ITM northing (m)
0.00000 0.00025 0.00050 0.00075 0.00100
normalised sensitivity
1.5 2.0 2.5 3.0
log10 (Ω m)

Figure 3.9: Line L6310 (Test Dataset B): Comparison between EM inversion resistivity models, normalised sensitivity sections and RMS errors computed (top three panels) using independent inversion (starting model for all sites is a 100 Ωm half-space) and (bottom three panels) non-independent inversion (starting model for each site is previous site's model, with the starting model for the first site on the line being a 100 Ωm half-space). Inversion regularisation parameters used in both cases are τ0 = 0.01 and τ1 = 2.894. The sensitivity normalisation factor used is the maximum sensitivity for the profile, determined separately for each profile. Horizontal blue line shows the mean RMS error for the profile. In both inversions, flight clearance data have been low-pass filtered (5-fiducial) and a PCA filter (k = 3) has been applied. Colour scale used has conductive bodies shown in red and resistive bodies in blues/purples. North is to the right-hand side of the profiles.

Results of the regularisation parameter tests, discussed in more detail further in the report, show that the tendency towards lateral discontinuity in the resistivity model sections produced by independent inversions can be significantly subdued by increasing the smoothness of the 1-D models (by increasing the value of parameter $\tau 1$) (Figure 3.10). Increasing $\tau 1$ also reduces the RMS misfit error for independent inversions and the value of $\tau 1 = 7.444$ used for the inversion of Figure 3.10 corresponds with the lowest average RMS error (equal to 1.086) for the resistivity section (see also Figure 3.12). However, there is some loss of vertical model resolution apparent when comparing the higher $\tau 1$ inversion of Figure 3.10 with the lower $\tau 1$ inversions of Figure 3.9. Thus, while laterally continuous, "non-blocky" models with low RMS errors may be obtained for independent inversions by employing higher $\tau 1$ values, it is achieved at the expense of vertical resolution. It is also noted that the lowest average RMS error achieved for the independent inversions (1.086 for $\tau 1 = 7.444$, model section of Figure 3.10) is slightly higher than that for the best non-independent inversion result (1.064 for $\tau 1 = 2.894$, model of Figure 3.9).

While independent and non-independent inversions produce models with similar RMS errors, and which are therefore quantitatively equally valid model solutions, the greater continuity of features in non-independent inversion models is preferred as being more geologically realistic and more interpretable. The trade-off between lateral continuity and vertical resolution required when employing independent inversions makes an independent inversion strategy less favourable. **On this basis non-independent inversions were used in the production inversion of the A6 Block**. Practically, there is some advantage in inversion time or speed in running non-independent inversions, as fewer inversion iterations are generally needed to converge on the final solution. However, this inversion speed advantage is offset by employing the strategy of

modelling each flight line twice, in forward and reverse directions (as discussed further in the section below).

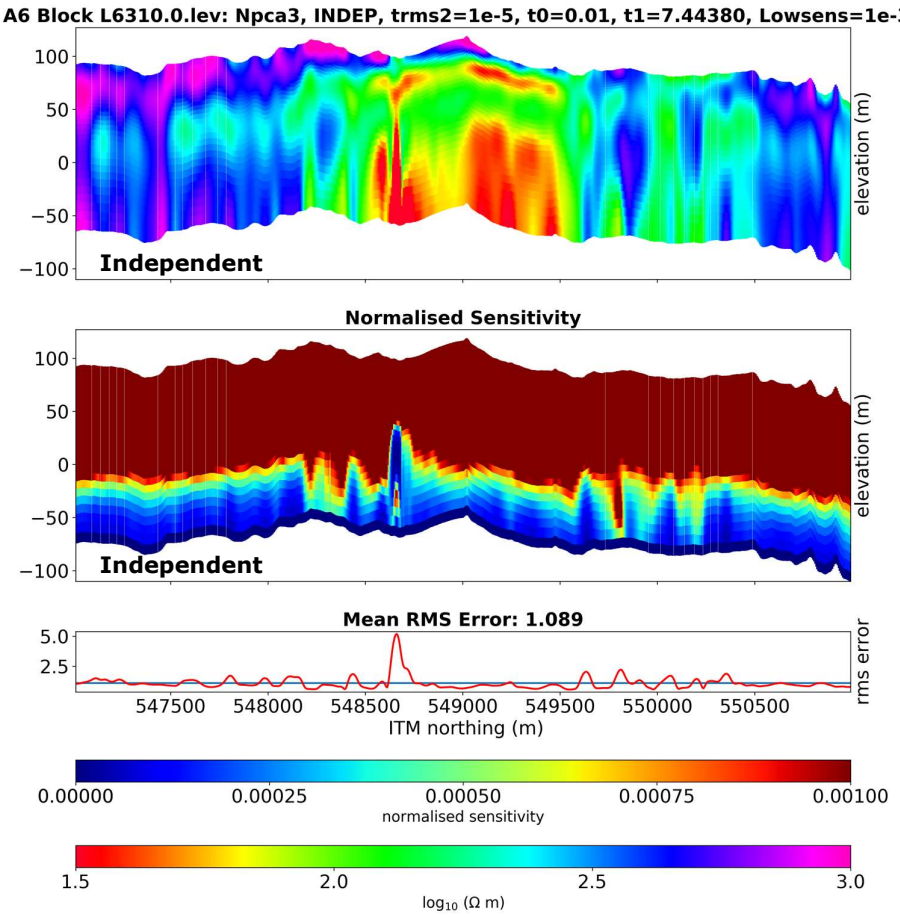

Figure 3.10: Line L6310 (Test Dataset B): EM inversion resistivity model, normalised sensitivity section and RMS errors computed using independent inversion (starting model for all sites is a 100 Ω.m half-space). Inversion regularisation parameters used are τ0 = 0.01 and τ1 = 7.444. The sensitivity normalisation factor used is the maximum sensitivity for the profile, determined separately for each profile. Horizontal blue line shows the mean RMS error for the profile. In both inversions, flight clearance data have been low-pass filtered (5-fiducial) and a PCA filter (k = 3) has been applied. Colour scale used has conductive bodies shown in red and resistive bodies in blues/purples. North is to the right-hand side of the profiles.

Averaging of Non-independent Inversion Models (FRA Strategy)

Running non-independent inversions (i.e., using the previous site's model as the starting model) raises the possibility that resulting model sections may be somewhat different depending on the line direction in which the inversions are run. It also presents the possibility of running inversions in both line directions, assessing the differences

between the two models and deriving an average model from two equally valid model solutions – a strategy referred to here as the "forward-reverse-average" (FRA) strategy.

The FRA strategy is examined below (Figure 3.11) using line L6311 model results from inversion Test 2 (Table 3.1) (Test Dataset A). The inversion data and parameter settings used are as follows: 5-fiducial low-pass filter applied to clearance data, Npca3 filter applied to EM component data, regularisation parameters $\tau 0$ = 0.01 and $\tau 1$ = 6.0, and data errors for all EM components = 60.0 ppm. The mean RMS errors for both line directions are practically identical: 0.985 for the forward direction inversion and 0.986 for the reverse direction.

While visually there are no significant differences apparent between the forward direction, reverse direction and average model sections in Figure 3.11, the percentage difference section does highlight portions of the model where the solutions might be regarded as less reliable. Note that percentage difference here is the percentage difference between the two models with respect to the average model, and is computed at every model depth location in the subsurface. Sites in the difference section, where large differences are seen throughout the vertical column, are generally coincident with high site RMS errors. In other instances, less stable model solutions (i.e., those solutions with larger differences) are only observed in deeper parts of the model.

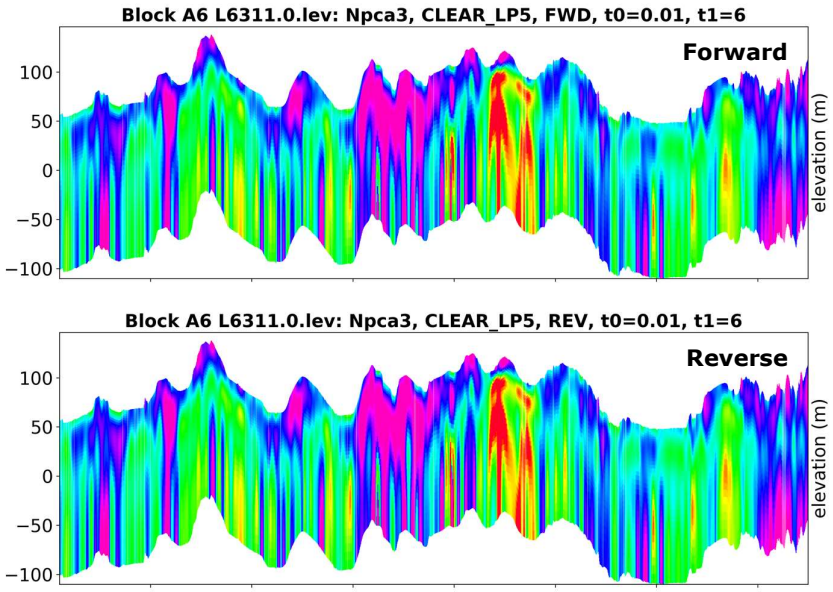

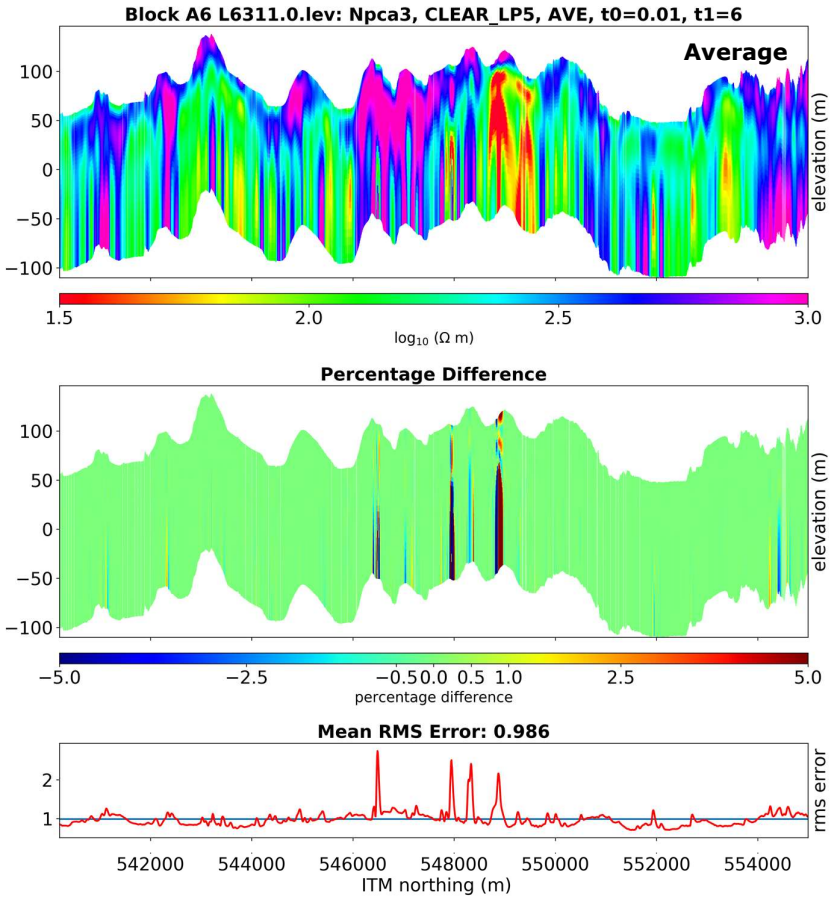

Figure 3.11: Line L6311 (Test Dataset A): Comparison between non-independent inversion models computed (top panel) in a forward direction along the profile and (second panel) in a reverse direction. (Third panel) shows the average of the forward and reverse direction models. (Fourth panel) shows the percentage differences between the two models with respect to the average model and (bottom panel) shows the average RMS error along the profile (i.e., average of forward and reverse direction RMS errors), with horizontal blue line indicating the line average. North is to the right-hand side of the profiles.

The percentage difference parameter provides an opportunity for rejecting poorer, less stable parts of the resistivity model, by defining an acceptable percentage difference threshold. Its application offers a more surgical approach than using site RMS error as a model rejection criterion – the latter rejecting the entire model associated with a site, while the former restricts rejection to specific portions and depths of the model section. The potential for automated, post-inversion model cleaning is seen as perhaps the main advantage of applying the FRA strategy, as the average resistivity models themselves are likely, in most cases, not to be significantly different from single direction inversion models.

The FRA inversion strategy has therefore been adopted for the production inversion of the A6 Block.

Inversion Regularisation Parameters

The values assigned to each of the two regularisation parameters associated with the *aempy* Tikhonov-type inversion have a particularly strong influence on the shape of the output resistivity models and on the closeness of the fit of the predicted EM responses to the observed responses (i.e., the model RMS error):

i. **τ0 parameter:** Controls the closeness of the inversion model to the *a priori* (starting) model (i.e., it controls the freedom to diverge from the starting model). Larger τ0 values allow less freedom to diverge from the starting model.

ii. **τ1 parameter:** Controls the 1-D model smoothness. Larger τ1 values produce smoother models.

The values that might be assigned to the regularisation parameters depend on the particular characteristics of the EM dataset being modelled (e.g., frequencies used and data errors) and on the parameterisation of the model space (e.g., number of layers, layer thicknesses and starting model). It is therefore necessary to run appropriate tests to determine the optimal values for parameters τ0 and τ1 for the dataset and inversion scheme being used.

For each of the two different versions of Test Dataset B used (one with 5-fiducial and the other with 20-fiducial low-pass filtered clearance data), four different tests (Table 3.1) were carried out to assess the effects of variation of τ0 (one test) and τ1 (three tests) on the output resistivity models and output RMS errors, for various different inversion inputs and schemes: independent and non-independent inversions and EM component data Npca3 filtered and not filtered. The clearance data are low-pass filtered (either 5-fiducial or 20-fiducial) for all tests. The tests evaluate τ0 in the range 0.001 – 1 (60 tests in total) and τ1 in the range 1 – 100 (40 tests in total), with logarithmic increments between each tau value tested. A task-specific *aempy* script was used to automate the tau test runs. All tests were run using data errors of 60.0 ppm for all eight EM components.

Figures 3.12 and 3.13 illustrate the tau versus model RMS error results ("L-curves") for a number of different test runs. The markedly different L-curve shapes, particularly for the $\tau 1$ tests (Figure 3.12), illustrate the importance of running the tests using the same inversion scheme and data errors as planned for production inversion.

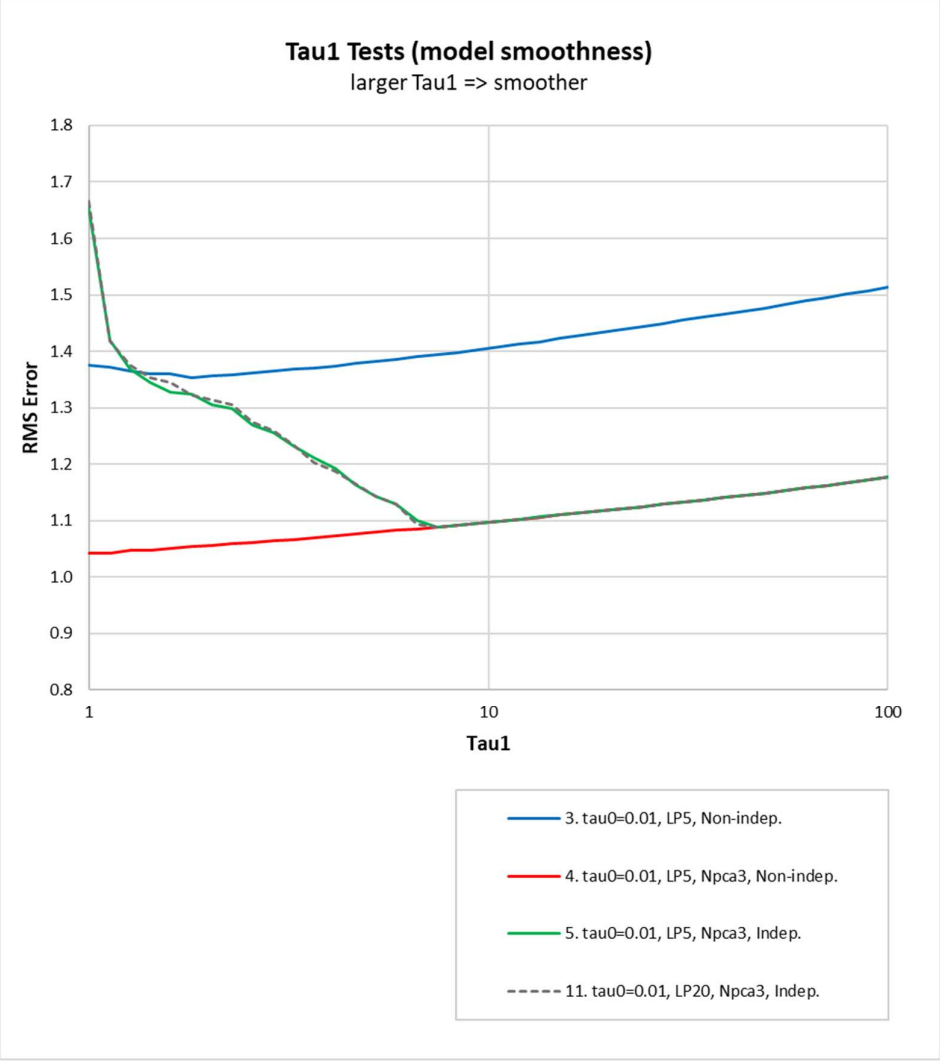

Figure 3.12: τ1 versus RMS error curves (L-curves) for a range of different τ1 tests (Line L6310, Test Dataset B). Primary details and settings for the tests are annotated in the legend and test numbers correspond with Table 3.1.

Test 4, running non-independent inversions with Npca3 filter applied to the EM responses, delivers the lowest RMS errors and with an L-curve characterised by a monotonic increase in RMS error from the lowest to highest $\tau 1$ values. The RMS error

reduction resulting from the application of the Npca3 filter, which removes noise elements in the EM data that cannot be well fit by the inversion models, is apparent in comparing Tests 3 and 4 in Figure 3.12. The independent inversion test (Test 5) shows a distinct minimum RMS error value at $\tau 1 = 7.444$, above which the shape of the RMS error curve replicates that of the non-independent inversions. Below $\tau 1 = 7.444$, the non-independent inversions always return lower RMS errors than the independent inversions.

The $\tau 0$ test (Figure 3.13) indicates that model RMS error is low with little sensitivity to changes in $\tau 0$ in the range 0.001 – 0.1. RMS error increases steadily with increasing $\tau 0$ above a value of 0.1, as the inversion models are held more strongly to the (poorer fitting) starting model.

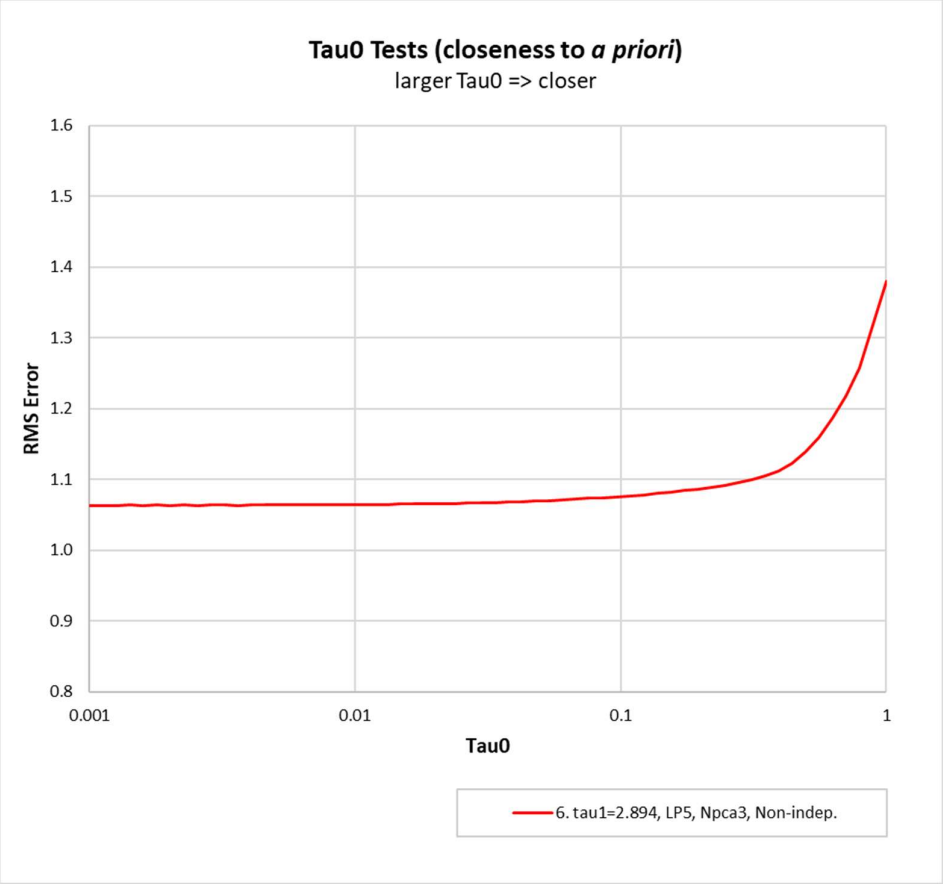

Figure 3.13: τ0 versus RMS error curves (L-curves) for a range of different τ0 tests (Line L6310, Test Dataset B). Primary details and settings for the tests are annotated in the legend and test numbers correspond with Table 3.1.

All L-curves shown in Figures 3.12 and 3.13 are for test runs in which a 5-fiducial low-pass has been applied to the clearance data. The 20-fiducial L-curves overlay almost exactly the 5-fiducial curves and have therefore not been plotted. Test 11 (20-fiducial filter), which is plotted in Figure 3.12, is the exception and shows very small RMS error variations with respect to Test 5 (5-fiducial filter) at $\tau 1$ values below 7.444. No appreciable difference in model RMS error results from applying either a 5-fiducial or 20-fiducial low-pass filter to the clearance data.

From a purely quantitative point of view, the best tau value is that providing the lowest RMS error model solution. For the tests most appropriate to the production inversion strategy used for the A6 Block (Test 4 for $\tau 1$, Figure 3.12 and Test 6 for $\tau 0$, Figure 3.13), the minimum RMS error tau values are: $\tau 0$ = 0.00112 and 0.00201 (RMS error = 1.063) and $\tau 1$ = 1.0 (RMS error = 1.042).

For the production inversion of the A6 Block, the following tau values were adopted:

$\tau 0$ = 0.01 and $\tau 1$ = 2.9

A strategic decision was taken to use the somewhat larger $\tau 0$ value of 0.01 for production inversion (which in Test 6 corresponds with an almost negligibly different RMS error of 1.065), rather than use the minimum RMS error $\tau 0$ values of 0.00112 or 0.00201, so as to encourage a moderately stronger adherence to the starting model (i.e., the previous site's model) and to (potentially) enhance model continuity along each flight line. Practically, however, the dependence of the output model "shape" on $\tau 0$ is very weak, particularly in the range of values between 0.001 and 0.1, as illustrated in Figure 3.14.

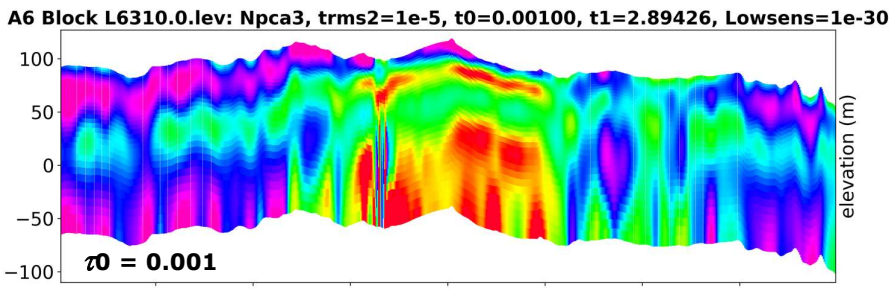

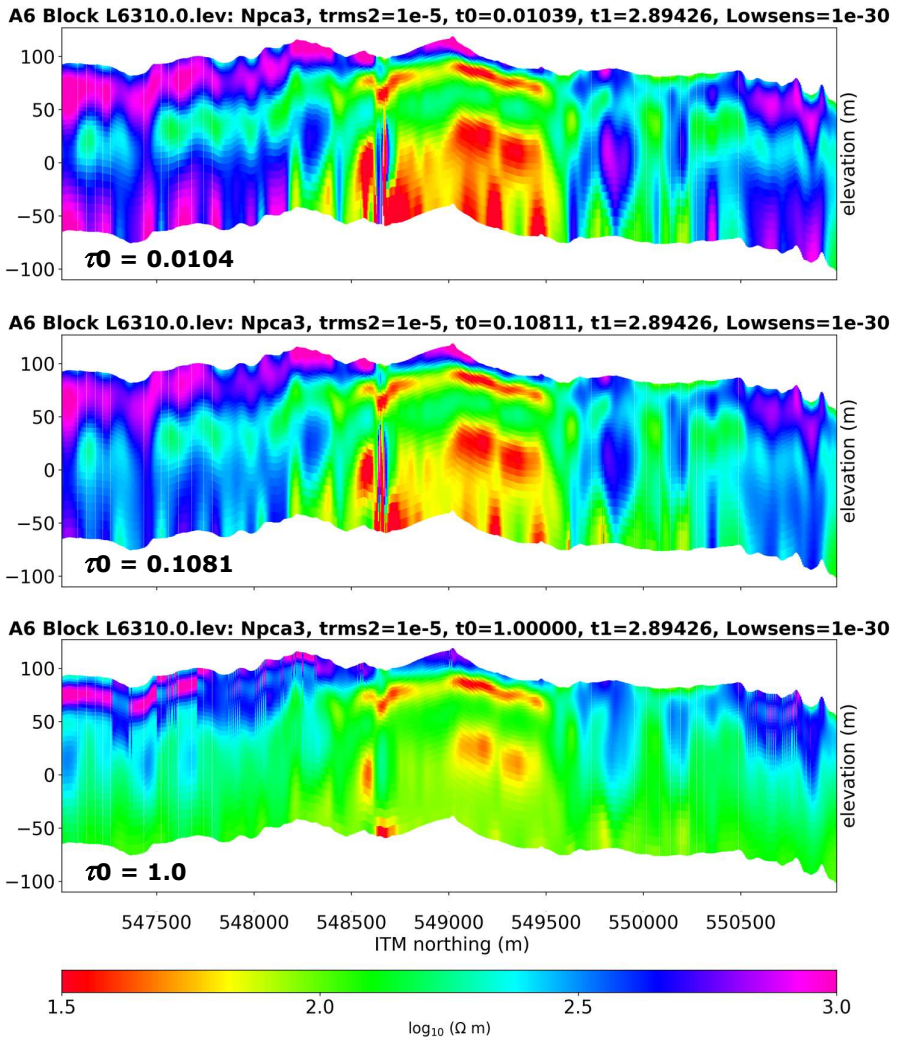

Figure 3.14: τ0 tests, Line L6310 (Test Dataset B): Comparison of output resistivity models for different inversion τ0 values, taken from Test 6 (Table 3.1). Figures from top to bottom illustrate results for τ0 values of 0.001, 0.0104, 0.1081 and 1.0 respectively. RMS errors for these models are 1.064, 1.065, 1.077 and 1.380 respectively. A value of τ0 = 0.01 was selected for production inversion of the A6 Block. North is to the right-hand side of the profiles.

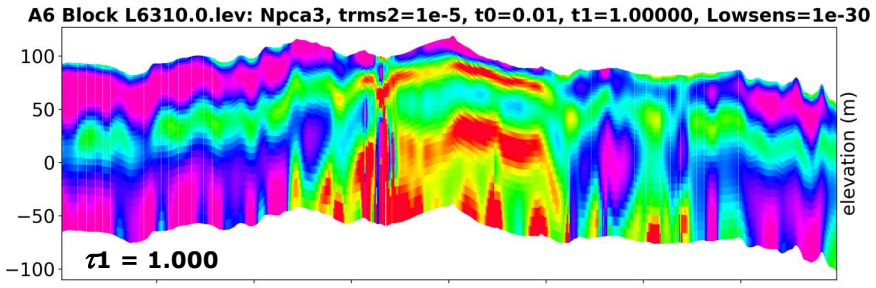

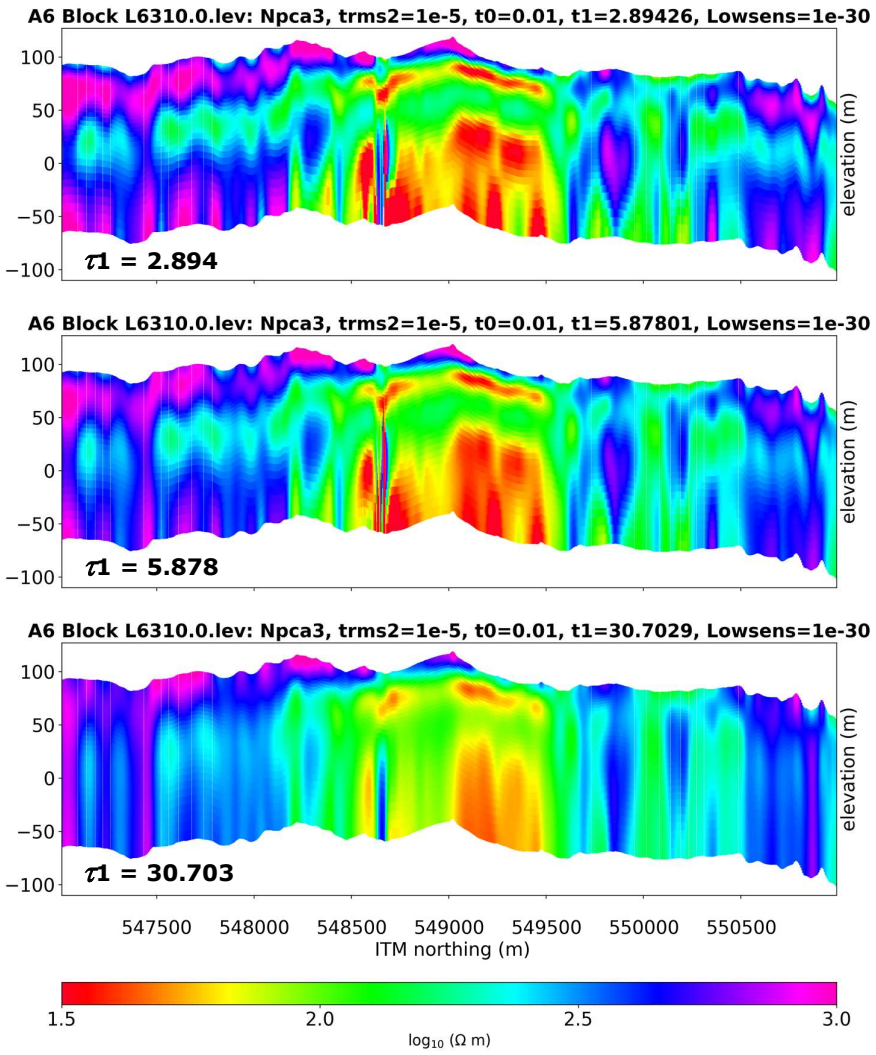

Figure 3.15: τ1 tests, Line L6310 (Test Dataset B): Comparison of output resistivity models for different inversion τ1 values, taken from Test 4 (Table 3.1). Figures from top to bottom illustrate results for τ1 values of 1.000, 2.894, 5.878 and 30.703 respectively. RMS errors for these models are 1.042, 1.064, 1.083 and 1.113 respectively. A value of τ1 = 2.9 was selected for production inversion of the A6 Block. North is to the right-hand side of the profiles.

The dependence of RMS error and model "shape" on $\tau 1$ is stronger than for $\tau 0$, as illustrated in Figure 3.15, with models becoming noticeably smoother (vertically) as $\tau 1$ increases, particularly above around $\tau 1 = 6.0$. The $\tau 1$ value of 2.9 was chosen for the production inversion of the A6 Block as there is an indication of slightly stronger lateral stability in the model section when compared with $\tau 1 = 1.0$. It corresponds with a negligible RMS error increase with respect to the minimum RMS error (1.042 for $\tau 1 = 1.0$ versus 1.064 for $\tau 1 = 2.894$) and shows little vertical resolution loss when compared with the $\tau 1 = 1.0$ model.

Other users of Tellus data and the *aempy* software may choose to use different $\tau 0$ and $\tau 1$ values from those used here for the production inversion of the A6 Block, so as to derive sharper or smoother models, depending on the geological setting and their modelling objectives.

EM Component Data Errors

Data errors estimated for and assigned to the eight EM data components (in-phase and quadrature for four frequencies 912, 3,005, 11,962 and 24,510 Hz) play a central role in controlling the inversion process and on output models generated by the inversion. Tikhonov-type inversion, as used by the *aempy* software, aims to converge on resistivity model solutions that fit the observed data to within their data errors. If data errors for all data components are the same, the inversion will aim to fit all components equally well. However, lower (or higher) errors assigned to a particular data component, will provide a stronger (or weaker) weighting towards fitting that component in the inversion. Assignment of data errors can therefore focus the inversion on different regions of the subsurface: for example, lower errors assigned to higher frequency data will tend to weight the inversion towards resolving shallower resistivity structure, and *vice versa* for lower errors assigned to lower frequency data and deeper structure. The *aempy* software allows data errors for all eight EM components to be assigned individually and separately.

A detailed analysis and assessment of the impact of different data error-sets on the output inversion models and model misfits was carried out prior to the inversion of the A5 Block and is reported on in the A5 Block inversion report (GSI, 2020a). A similar assessment has not been reproduced for the A6 inversion. The findings of the A5 Block assessment, summarised below, have been followed for A6, leading to the **assignment of 60.0 ppm data errors to all data components for the A6 inversion**, the same as used for Block A5.

The A5 Block error tests examined a number of different error sets, consisting of various hypothetical errors and errors derived from the statistical analysis of high-fly data recorded over the Tellus Bundoran test line and within the A5 Block itself, and providing a range of different relative weightings of the four frequencies and eight components in

the EM data. Output models from the A5 tests were assessed by: (i.) qualitatively, examining resolution and depths of investigation in the models and (ii.) quantitatively by examining the data misfit residuals (in ppm) for all eight EM data components, where:

$$misfit\ residual = predicted\ model\ response - observed\ response \quad (5)$$

Misfit residuals (and their absolute values) are a more useful metric for test comparison purposes than RMS error. Misfit residuals reflect absolute differences between the predicted and observed responses (separately for each of the eight data components) and are "signed" (positive where the predicted responses are higher than the observed, and negative where lower). Model RMS errors reflect a misfit dependent on the data errors themselves (as the residuals are normalised by the data error in computing RMS error), are not "signed" (as the residuals are squared), and in summing all eight data components' residuals together, lose information about the fit of individual components.

The average of the eight component means of the residual absolute values (see, e.g., the residuals for the A6 production inversions, Table 4.3 below) was used as a measure of the overall quality of fit for each A5 Block error-set test. These averages indicated very similar overall qualities of fit for all error-sets, and further showed that changing the relative magnitudes of data error between different components (and therefore changing the relative weighting of the components in the inversion) redistributes the misfits between the components, without affecting the overall quality of fit for the entire dataset. Examination of the impacts on the output resistivity models of the different A5 error-sets indicated that where higher frequencies are preferentially weighted (with lower data errors), there is some enhancement in the strength and continuity of shallow and mid-level (~25 m depth) conductors, but at the expense of loss of sensitivity to deeper resistors in the model. Conversely, where lower frequencies are preferentially weighted with lower data errors, imaging of deeper resistive structures is enhanced, but with significant degradation of the surficial and mid-level conductors in the model. Unweighted errors of 60.0 ppm for all EM data components were judged to provide a reasonable compromise between shallow and deep imaging in the A5 Block test models and were adopted for the A5 production inversions. The same errors have been used for the A6 Block inversions.

4. Data Inversion

Inversion Parameters

Guided by the inversion tests reported on in Section 3, Tikhonov-type 1-D inversions were run on the full A6 Block dataset, on a line-by-line basis, using non-independent inversions coupled with the forward-reverse-average (FRA) strategy, in which models are computed in forward and reverse directions along each line and subsequently averaged. Inversion parameters and workflow are summarised in Table 4.1. Logarithmically increasing layer depths for the 35 layers used in the inversion are specified in Table 4.2.

The *aempy* software was run on a Windows 10 laptop computer, running *Python* (using the *Spyder* Integrated Development Environment) under *Ubuntu Linux* within an *Oracle VM VirtualBox*. The laptop specifications are: Intel i7-8850H CPU @ 2.60 GHz, 32 GB RAM (with 16 GB virtual memory allocated to the virtual machine).

A summary of several inversion statistics are reported below:

i. Number of lines inverted: 465 (traverse lines only, no tie-lines inverted).

ii. Total number of sites inverted: 2,145,192.

iii. Inversion time: 173 runtime hours.

Table 4.1. Inversion parameters and workflow. Amongst the data channels imported into aempy are: "MSLHGT", the aircraft GPS Z coordinate referenced to mean sea level and "PLM_nT", the power line monitor (the latter imported into aempy, but not used).

PROCESSING STEP	SOFTWARE	PARAMETERS AND COMMENTS
Pre-processing		
Data import	*Geosoft*	Import into *Geosoft*. Input data file: [GSI___18.IRL_DLV2159_FEM.xyz]
Smoothing of laser altimeter data	*Geosoft*	Low-pass filter, 5-fiducial.
Data export	Geosoft	Export data channels required by *aempy*: line name, ITM_X, ITM_Y, MSLHGT, RADAR_LP20, In-phase 0.9 to 25 kHz, Quadrature 0.9 - 25 kHz, PLM_nT.
Data import	*aempy*	Import into *aempy* software.

De-noising of EM data	*aempy*	Principal Component Analysis filter (Npca3 filter, retaining singular values 1, 2 and 3).
Tikhonov-type 1D regularised inversion		
Data inversion on a line-by-line, site-by-site basis	*aempy*	Number of layers (excluding final half-space): 35
		Layer thickness: increasing logarithmically, 2.0 m at surface to 9.6 m at 170 m depth.
		Starting model for first site on line: 100 Ω.m half-space.
		Starting model for all other sites on line: previous site's 1-D model.
		Inversion direction on line: forward and reverse directions (i.e., two inversions per site).
		$\tau 0$ regularisation parameter (closeness to starting model): 0.01
		$\tau 1$ regularisation parameter (model smoothness): 2.9
		Data errors: 60.0 ppm for all 8 EM data components.
Model averaging	*aempy*	Compute average of forward and reverse direction runs: resistivity model, RMS errors, predicted EM responses and percentage difference between two models with respect to average model.
Data output	*aempy*	Output in *Geosoft* .XYZ format: model resistivity, model percentage difference, model sensitivity (all three parameters sorted into depth channels), RMS error, predicted and observed EM responses for 8 components.

Table 4.2. Model layer depths used in inversion of the A6 Block EM data (depths recorded correspond with depth at the mid-point of the layer).

Depth Layer	D1	D2	D3	D4	D5	D6	D7	D8	D9
Depth (to mid-layer) (m)	1.0	3.0	5.2	7.4	9.8	12.3	14.9	17.6	20.5

Depth Layer	D10	D11	D12	D13	D14	D15	D16	D17	D18
Depth (to mid-layer) (m)	23.4	26.6	29.9	33.3	36.9	40.7	44.7	48.9	53.2

Depth Layer	D19	D20	D21	D22	D23	D24	D25	D26	D27
Depth (to mid-layer) (m)	57.8	62.6	67.7	72.9	78.5	84.3	90.4	96.7	103.4

Depth Layer	D28	D29	D30	D31	D32	D33	D34	D35	

Depth (to mid-layer) (m)	110.4	117.8	125.5	133.6	142.1	150.9	160.3	169.8	

Evaluation of Models and Fit

A range of different QC parameters are presented and considered here in assessing the reliability of the inversion models and their closeness of fit to the observed EM responses: site RMS error, misfit residuals, model percentage differences (between the forward and reverse line direction inversion models) and model sensitivity. Direct visual comparisons between observed and predicted EM responses are not presented here but may be found in Section 5 ("Model Cleaning").

An example model-output from the *aempy* inversions is shown in Figure 4.1, where the resistivity solutions for the 29.9 m depth layer are gridded and mapped across the survey area. A reassuring outcome of the modelling is that while the inversions were run independently on a line-by-line basis, there is nevertheless very good line-to-line continuity of geological features. Spatial resolution of the resistivity features also matches well the spatial variation observed in maps of the eight EM data components. High-fly areas are clearly recognised as anomalously high conductivity areas in the resistivity map, a result of the inversions returning (spurious) conductive bodies given, as input, very low EM component amplitudes and high flight heights.

Note that in this section of the report, the (lower) maps in Figures 4.1, 4.2 and 4.4 – 4.7 are presented with data blanked (nulled) where flight clearance > 120 m. The data blanking is carried out for presentation purposes only, to illustrate a spatial coincidence between poor model QC parameter responses and high-fly areas. Similarly, the inclusion of the data-subset with clearance < 120 m in the model misfits and statistics presented in Table 4.3 and Figure 4.3 is intended only to illustrate the potential impact of high-fly areas on average model misfits. The "production" rejection of poor inversion model solutions ("model cleaning") is carried out using thresholds assigned to three selected QC criteria, rather than using a universal flight clearance threshold, as presented and discussed in Section 5.

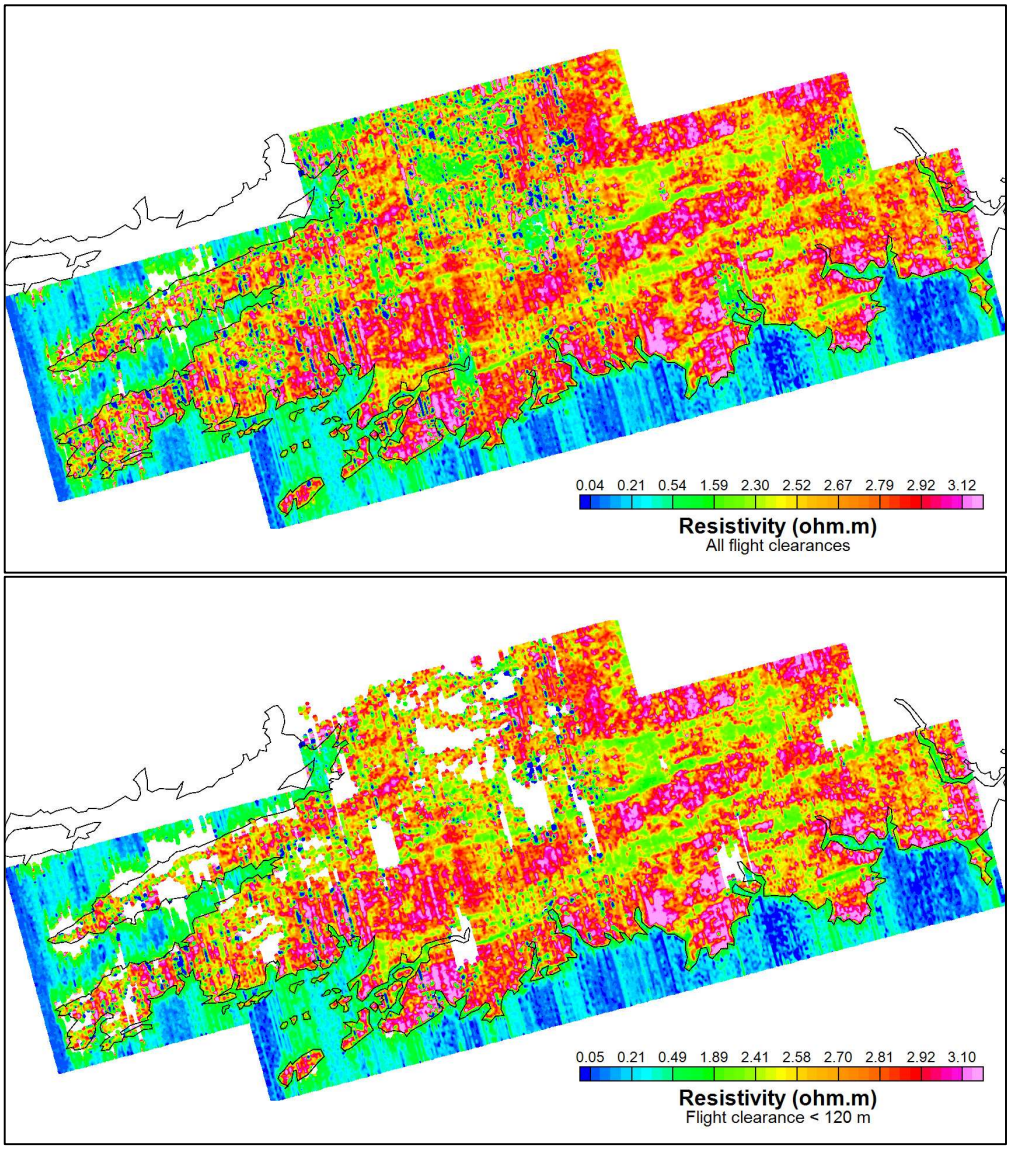

Figure 4.1: A6 Block EM inversion – grid maps of resistivity for the 29.9 m depth layer in the inversion models. (Top) full dataset. (Bottom) dataset blanked where flight clearance > 120 m. Grid: Inverse Distance Weighted with 50 x 50 m grid mesh. Colour scale used: equal area distribution on logarithmic scale, with conductors shown in blue and resistors in red. Irish coastline shown (black line). (Note: data blanked in lower figure for illustrative purposes only. Rejection of poor model solutions is discussed in Section 5).

RMS Errors

RMS error provides a broad indication of the quality of the fit of the models to the observed data, with respect to the data errors. An RMS error equal to one indicates that the observed data are fit to within their data errors. Average RMS error statistics for the A6 Block inversion are as follows:

- **Mean RMS error = 1.916.** Standard Deviation = 3.588, total number of sites = 2,145,192.

- **Mean RMS error for clearance < 120 m = 1.388.** Standard Deviation = 3.575, total number of sites = 1,796,925 sites (83.8% of A6 total).

Figure 4.2: A6 Block inversion – grid maps of site RMS error. (Top) full dataset. (Bottom) dataset blanked where flight clearance > 120 m. Grid: Inverse Distance Weighted with 50 x 50 m grid mesh. Linear colour scale used. Irish coastline shown (black line). (Note: data blanked in lower figure for illustrative purposes only. Rejection of poor model solutions is discussed in Section 5).

The significantly lower mean RMS error calculated for sites with flight clearance < 120 m indicates that a large proportion of the poor model solutions are associated with high-fly areas – as further illustrated in Figure 4.2, where, in the lower figure, data with flight clearance > 120 m are blanked. In addition to high RMS errors associated with high-fly areas, there are also several individual lines, or portions of lines where RMS error is relatively high, as well as lineaments associated with power-line or other cultural noise.

Misfit Residuals

Analysis of misfit residuals (Equation 5) for all eight EM data components, for both the full A6 dataset and the data subset with flight clearance < 120 m (Table 4.3 and Figure 4.3), indicates that the best fit EM components are in-phase and quadrature at 0.9 and 3 kHz. The poorest fit corresponds with the 12 kHz quadrature component. Average misfit residuals are appreciably reduced by the exclusion of high-fly data for both in-phase and quadrature components at 12 and 25 kHz, as well as for the quadrature component at 3 kHz (Figure 4.3). Computing the average of the eight component means of the absolute value residuals (Table 4.3) provides a measurement of the overall quality of fit for the A6 inversion: 84.9 ppm for the full dataset and 60.6 ppm for the low-fly data subset. The latter misfit figure is very similar to the 60.0 ppm error assigned to the data, suggesting that the error assignment is of the right order. In comparison with the 67.0 and 63.2 ppm eight-component residual absolute value means for the A5 and WFD Blocks (Table 4.3), the A6 Block (low-fly) data are on average moderately better fit.

Table 4.3: A6 Block inversion misfit residuals: Means of residuals and means of absolute values of residuals for all eight EM components. Data presented for full dataset and dataset where clearance < 120 m. In the case of absolute value data, a mean across all eight data components is computed, providing an overall measurement of the quality of fit for the dataset. Negative residual values are highlighted in red (where amplitude of predicted response is lower than observed response). The total number of sites for the full A6 dataset 2,145,192, and for the subset with clearance < 120 m, 1,796,925. Statistics for the WFD (Waterford) Block (861,015 data) and A5 Block (3,177,858 data) for clearance < 120 m are recorded for comparison.

Dataset	Mean (ppm)	P09 Mean (ppm)	P3 Mean (ppm)	P12 Mean (ppm)	P25 Mean (ppm)	Q09 Mean (ppm)	Q3 Mean (ppm)	Q12 Mean (ppm)	Q25 Mean (ppm)
Absolute values of residuals									
A6 Full dataset	**84.9**	48.8	71.6	74.2	122.9	34.5	62.0	168.6	96.9
A6 Clear. < 120 m	**60.6**	42.6	64.5	47.8	79.0	30.7	40.3	114.5	65.6

WFD Clear. < 120 m	**63.2**	58.9	52.7	76.3	62.6	40.2	53.0	96.4	65.3
A5 Clear. < 120 m	**67.0**	41.0	44.2	81.0	125.3	45.1	52.0	86.8	61.0

Residuals									
A6 Full dataset		7.7	-34.9	-11.4	-36.4	2.1	-55.8	-155.4	-33.5
A6 Clear. < 120 m		1.1	-37.0	22.5	23.3	11.1	-33.1	-98.7	9.9
WFD Clear. < 120 m		-21.3	16.6	-7.5	38.9	-0.6	-27.4	-83.7	45.2
A5 Clear. < 120 m		-4.7	-0.5	-49.6	112.9	13.3	-28.6	-69.4	-38.1

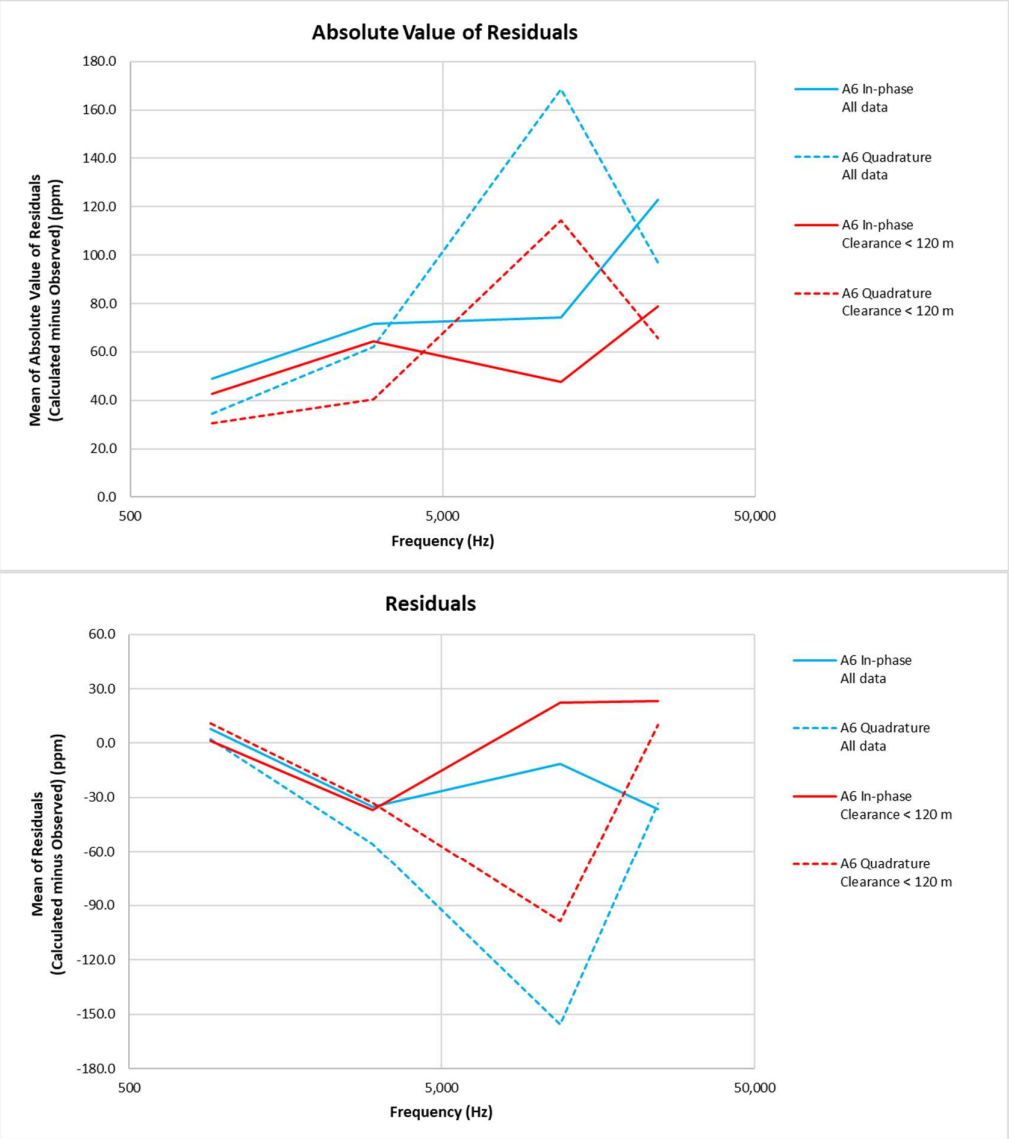

Figure 4.3: A6 Block inversion misfit residuals: (Top) Mean of absolute values of residuals plotted for all 4 frequencies for in-phase and quadrature components. (Bottom) Mean of residuals plotted for all 4 frequencies for in-phase and quadrature components. Analysis for all data shown (in blue) and for data where flight clearance < 120 m (in red).

Examining the means of the residuals for each data component (Figure 4.3, bottom panel, and Table 4.3) provides an indication of the match between the average "baselines" of the predicted and observed responses. For A6, the observed baselines are all reasonably well matched (to within ±40 ppm for the low-fly data) for all components, except for the quadrature component at 12 kHz (-98.7 ppm average misfit, predicted response lower in amplitude than observed response).

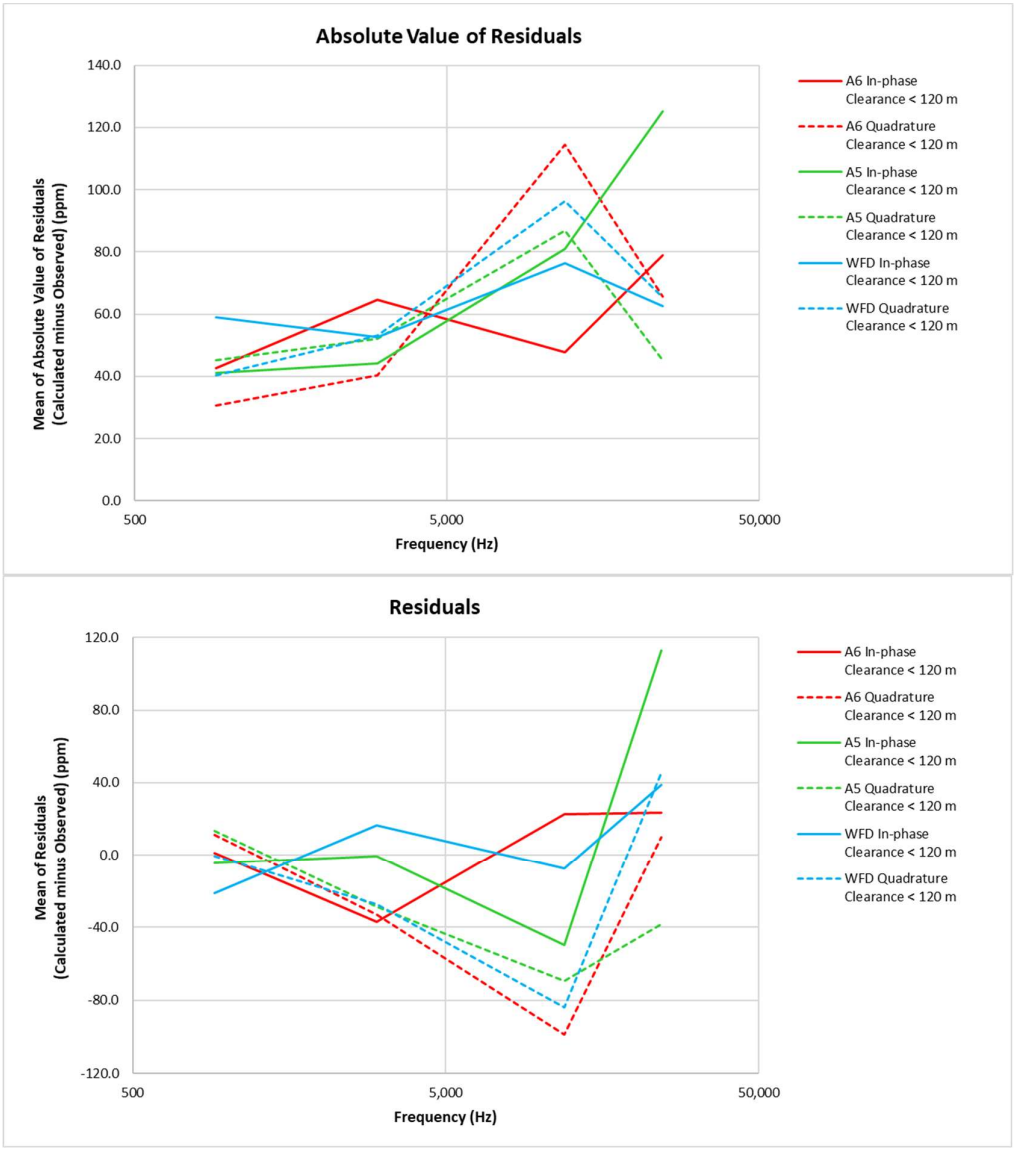

Figure 4.4: A6 Block inversion misfit residuals (red) in comparison with residuals for A5 (green) and WFD (blue) Block inversions, for data where flight clearance < 120 m: (Top) Mean of absolute values of residuals plotted for all 4 frequencies for in-phase and quadrature components. (Bottom) Mean of residuals plotted for all 4 frequencies for in-phase and quadrature components.

Figure 4.4 compares the means of residuals and means of absolute values of residuals for all 3 EM inversion survey blocks completed to date. It is apparent, in examining the means of residuals within each survey area, that the inversion models are unable to match simultaneously the observed baselines of all EM data components simultaneously: for example, the 12 kHz and 25 kHz quadrature components in the WFD Block and the 12 kHz and 25 kHz in-phase components in the A5 Block. In comparing the means of the residuals, and therefore the observed data baselines, across survey blocks, there are similarities in some components: for example, the observed 3 kHz quadrature component is generally ~30 ppm higher on average than the predicted responses, and the 12 kHz quadrature component is generally ~80 ppm higher. The other data component baselines are variably higher or lower on average than the predicted responses from survey block to survey block. Further consideration of possible imbalances between the baselines of the observed data components, both within survey blocks and from survey block to survey block, is beyond the scope of this current inversion work and report. However, as the component data baselines are retrospectively updated for consistency across all survey bocks by contractor SGL on completion of each new Tellus block, there may be scope for using the average misfit residual statistics from each completed inversion block as an additional constraint on the work.

The spatial distribution of misfit residuals (absolute value), exemplified by that of the in-phase 12 kHz residuals (Figure 4.5), confirms a correlation between high residual values and high-fly areas. Blanking the residuals for flight clearances > 120 m (lower panel, Figure 4.5) removes a large number of the high-residual data points. There are several individual lines, or portions of lines where high residual values are apparent, as well as lineaments associated with power-line or other cultural noise.

Figure 4.5: A6 Block inversion – grid maps of absolute values of misfit residuals for in-phase 12 kHz component (Top) full dataset. (Bottom) dataset blanked where flight clearance > 120 m. Grid: Inverse Distance Weighted with 50 x 50 m grid mesh. Linear colour scale used. Irish coastline shown (black line). (Note: data blanked in lower figure for illustrative purposes only. Rejection of poor model solutions is discussed in Section 5).

Model Percentage Difference

A further parameter from the inversion process that allows assessment of model quality and reliability is the percentage difference between the forward and reverse line direction inversion models. Similar to RMS error and misfit residuals, a correlation is observed between high-fly areas and large model percentage differences, as illustrated

in Figure 4.6 for the case of the 29.9 m depth layer from the inversion models. In addition, there is also a clustering of large model percentage differences (greater than ±5%) observed in the map along the Cork coastline. It appears that the non-independent inversion models, using the previous site's response as the starting model, do not respond immediately to the very rapid lateral transition in resistivity properties on the coastline, with different model solutions arising on the coastline depending on the direction of inversion across the coastline. In addition, there are lines, or portions of lines where high percentage differences are apparent, as well as several lineaments associated with power-line or other cultural noise.

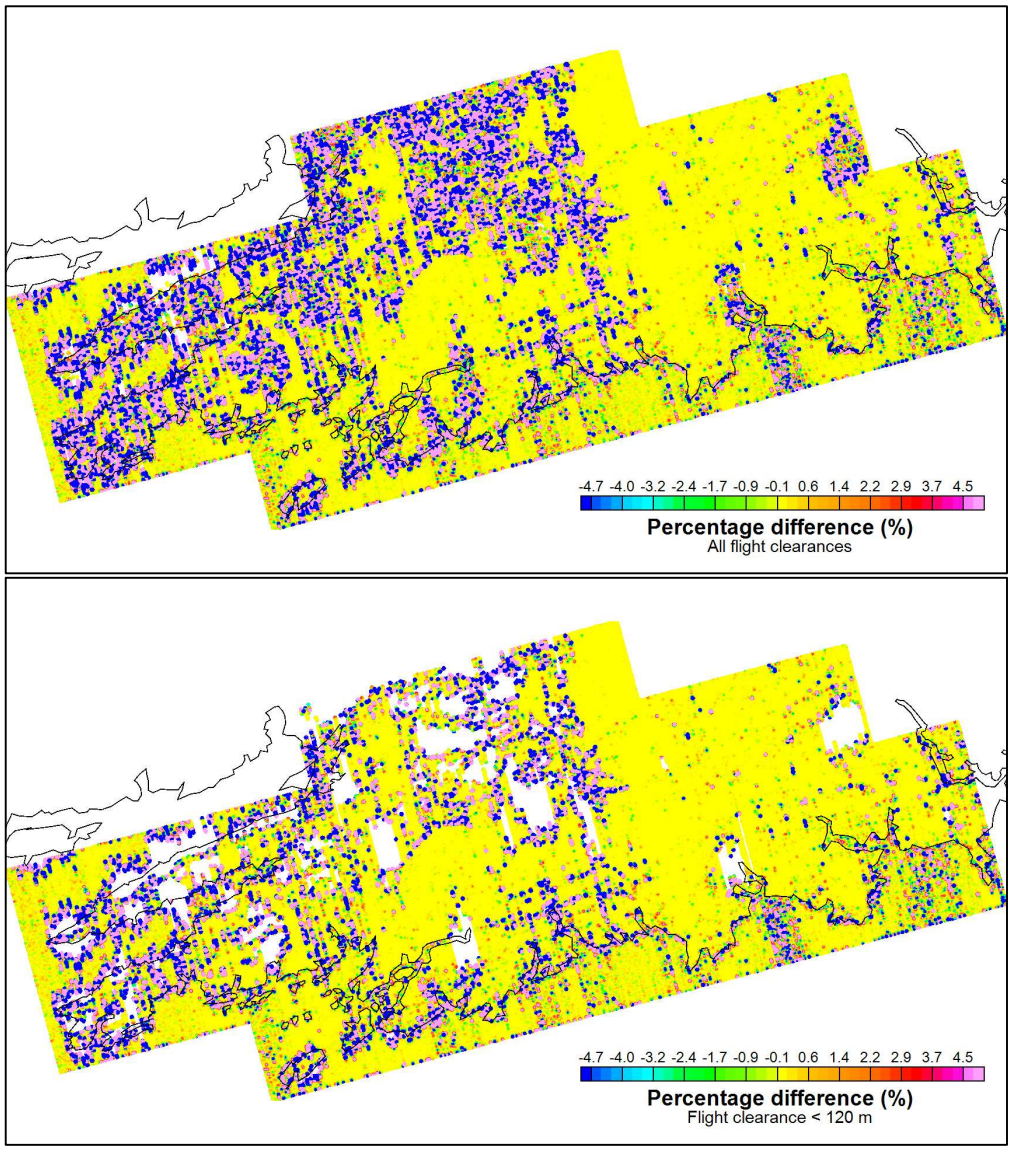

Figure 4.6: A6 Block inversion – grid maps of resistivity model percentage difference for 29.9 m depth layer (Top) full dataset. (Bottom) dataset blanked where flight clearance > 120 m. Grid: Inverse Distance Weighted with 50 x 50 m grid mesh. Linear colour scale used. Irish coastline shown (black line). (Note: data blanked in lower figure for illustrative purposes only. Rejection of poor model solutions is discussed in Section 5).

Model Sensitivity

A marked reduction in model sensitivity is apparent in high-fly areas, as illustrated in the example of the 29.9 m model depth layer in Figure 4.7. The model sensitivities have been normalised by the average sensitivity of the shallowest model layer, at 1.0 m depth, as explained further in Section 5. Conductive geological bodies in the subsurface are characterised by high sensitivities – hence the observed (inverse) correlation between the model sensitivity map and the resistivity map of Figure 4.1.

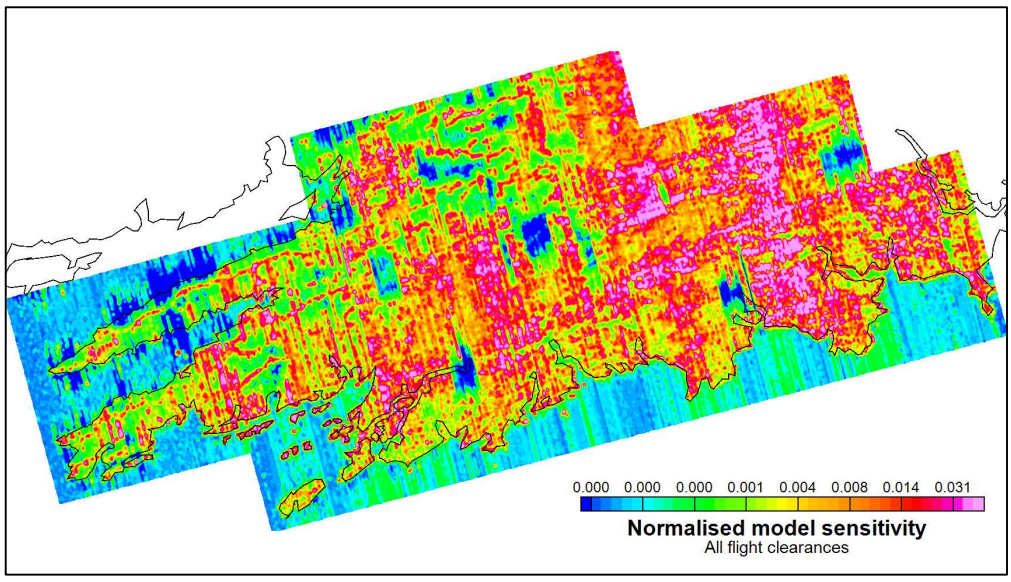

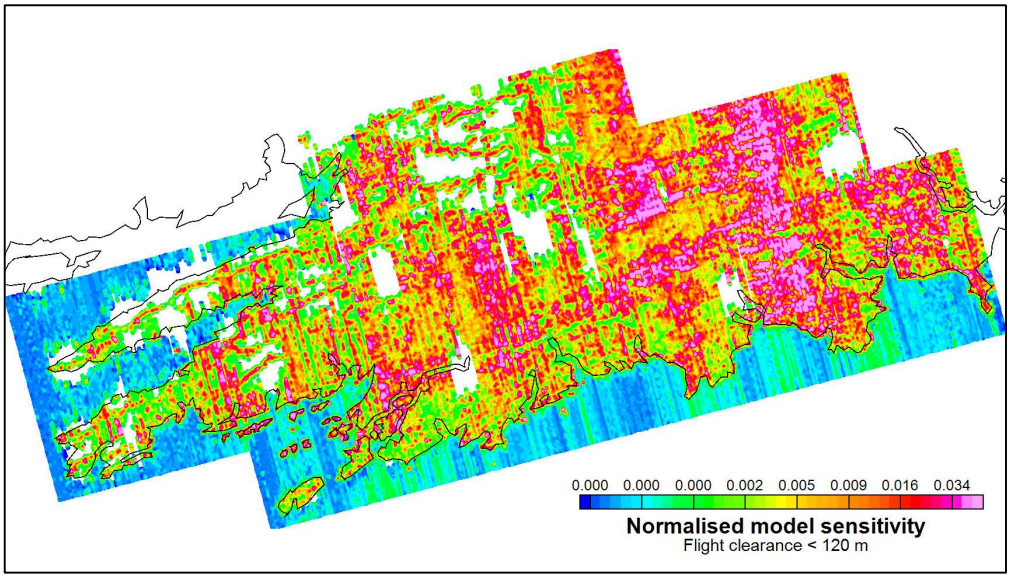

Figure 4.7: A6 Block inversion – grid maps of normalised model sensitivity for 29.9 m depth layer (Top) full dataset. (Bottom) dataset blanked where flight clearance > 120 m. Model sensitivities are normalised by the average sensitivity of the shallowest model layer, at 1. 0 m depth, for the full dataset. Grid: Inverse Distance Weighted with 50 x 50 m grid mesh. Colour scale used: equal area distribution. Irish coastline shown (black line). (Note: data blanked in lower figure for illustrative purposes only. Rejection of poor model solutions is discussed in Section 5).

The offshore portion of the survey area is characterised by very low model sensitivities in the 29.9 m model depth layer, a result of the much reduced skin depths (depths of investigation) associated with the very high seawater conductivity. Skin depths (Equation 1) for seawater of nominal resistivity 0.25 Ω.m, for each of the 0.9, 3, 12 and 25 kHz transmission frequencies, are 1.6, 2.3, 4.6 and 8.3 m respectively, resulting in very high model sensitivities in the shallowest 1.0 m depth layer (Figure 4.8) where constraints are provided by all four frequencies. A rapid reduction in sensitivity with depth follows, as the constraints offered by the higher frequencies fall away. Minimal model sensitivity persists in seawater below around 10 m depth.

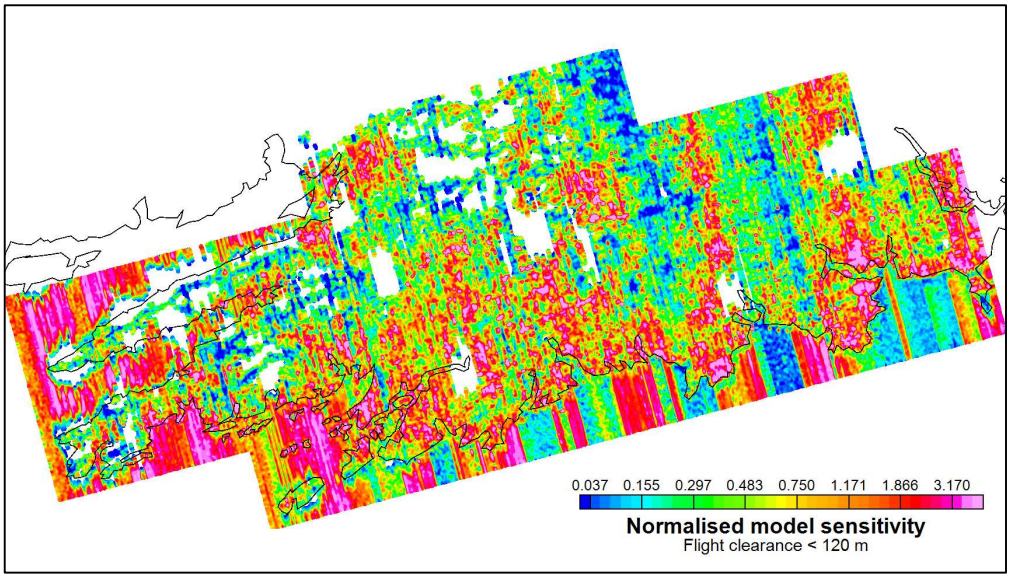

Figure 4.8: A6 Block inversion – grid map of normalised model sensitivity for 1.0 m depth layer, with dataset blanked where flight clearance > 120 m. Model sensitivities are normalised by the average sensitivity of the shallowest model layer, at 1.0 m depth, for the full dataset. Grid: Inverse Distance Weighted with 50 x 50 m grid mesh. Colour scale used: equal area distribution. Irish coastline shown (black line). (Note: data blanked in lower figure for illustrative purposes only. Rejection of poor model solutions is discussed in Section 5).

Summary

There is a clear association between poor QC parameter responses and low model sensitivity, and high-fly areas and sources of cultural noise. Loss of geological signal strength with increasing flight clearance is dependent on the subsurface resistivity structure itself, with conductive and/or shallow bodies retaining signal strength to higher clearances than resistive and/or deeper ones. Using a universal flight clearance threshold as a model rejection criterion therefore runs the risk of rejecting reliable parts of the model if the clearance threshold is set too low, and retaining unreliable parts of the model if the threshold is set too high. Flight clearance rejection will also not address poor model solutions due to cultural noise in low-fly areas. Rather than using a broad-brush flight clearance threshold for model cleaning, a number of the QC parameters discussed in this section have been applied, with appropriate thresholds, to reject poor model solutions – as discussed in Section 5 below.

5. Model Cleaning

The objective of "model cleaning" is to remove poor solutions from the models, primarily those associated with high-fly zones where geological signal strength is low, but also those resulting from cultural noise. Model cleaning was carried out within *Geosoft Oasis Montaj* software. Inversion resistivity models and supporting QC parameters, produced by *aempy*, were exported as ascii files in a format suitable for import into *Geosoft* (*Geosoft* .XYZ format). The model data for all sites remain in flight-line order, and resistivity values for each depth layer appear as separate resistivity channels when imported into a Geosoft database. Table 5.1 summarises the data channels exported from *aempy* and imported into *Geosoft*.

Table 5.1. List of data channels exported from aempy and imported into Geosoft software.

Data channels	Units	Description
LINE	-	Line number
ITM_X	m	X coordinate: IRENET95 ITM
ITM_Y	m	Y coordinate: IRENET95 ITM
DEM	m	Digital elevation model (referenced to sea level)
ALT	m	Flight clearance
P09npca3 to P25npca3	ppm	Observed in-phase 0.9 kHz to 25 kHz response (4 components, Npca3 filtered)
Q09npca3 to Q25npca3	ppm	Observed quadrature 0.9 kHz to 25 kHz response (4 components, Npca3 filtered)
P09calc to P25calc	ppm	Predicted in-phase 0.9 kHz to 25 kHz response (4 components)
Q09calc to Q25calc	ppm	Predicted quadrature 0.9 kHz to 25 kHz response (4 components)
RMSErr	-	Site RMS error
ResD1.0 to ResD169.8	$\log_{10}$ (ohm.m)	Model resistivity for 1.0 m depth layer to 169.8 m depth layer (35 depth layers)
QCpdiffD1.0 to QCpdiffD169.8	%	Model percentage difference for 1.0 m depth layer to 169.8 m depth layer (35 depth layers)
SensD1.0 to	ppm/ log10	Model sensitivity for 1.0 m depth layer to 169.8 m depth layer

SensD169.8	(ohm.m)	(35 depth layers)

The model cleaning work flow is summarised in Table 5.2, together with the parameters and QC thresholds selected and used. The workflow was established by examination of the characteristics of different types of noise in the models and their correlations with the QC parameters derived from the *aempy* inversion. All operations were performed with resistivity values expressed as $\log_{10}$(resistivity). In the discussion that follows, for ease of expression, each depth layer is referred to in the form "D*n*", where *n* is the depth to the mid-point of the layer. For example, D1.0 and D29.9 refer to model layers at depths of 1.0 m and 29.9 m respectively. Thirty-four depth layers from D1.0 to D160.3 were processed through the initial two stages of the work flow, QC parameter threshold rejection, and smoothing and interpolation. Twenty-seven depth layers from D1.0 to D103.4 were passed on to the next stage, microlevelling, and subsequently the shallowest twenty depth layers to D62.6, assessed as robust and well constrained, were exported in several different data formats for public release.

Table 5.2. Model cleaning workflow and parameters. Depth layers are referred to in the form "Dn", where n is the depth to the mid-point of the layer (e.g., D1.0 and D29.9 refer to model layers at depths of 1.0 m and 29.9 m respectively).

PROCESSING STEP	SOFTWARE	PARAMETERS AND COMMENTS
1. QC parameter threshold rejection (depth-by-depth, line-by-line basis)		
Normalise model sensitivity.	*Geosoft*	Normalise sensitivity (by division) using D1.0 whole-dataset average sensitivity = 93.9495.
Apply normalised sensitivity (Nsens) threshold.	*Geosoft*	Apply only where flight clearance > 90 m.
		Reject model solution where sensitivity < sensitivity threshold. Depth dependent thresholds, using $\log_{10}$-linear interpolation between the following tie-points: D1.0 = 0.5, D5.2 = 0.05, D9.8 = 0.005, D20.5 = 0.0025, D29.9 = 0.0015, D44.7 = 0.00075, D62.6 = 0.0003, D103.4 = 0.00015. For D103.4 to D160.3 = 0.00015.
Apply model percentage difference (QCpdiff) threshold.	*Geosoft*	Reject model solution where QCpdiff > 5% or QCpdiff < -5%.
Apply 12 kHz in-phase residual (P12resid) threshold.	*Geosoft*	Reject model solution where P12resid < -131.4 ppm or P12resid > 108.6 ppm (effectively a data mismatch greater than ±120 ppm, allowing for mean residual for whole dataset of -11.4 ppm, Table 4.3).
2. Smoothing and Interpolation		

Smoothing of models on a line-by-line basis, for each depth layer.	*Geosoft*	Low pass filter, 10-fiducial.
Reject outlier model resistivities.	*Geosoft*	Reject model solution where $\log_{10}$(resistivity) < -1.0 or $\log_{10}$(resistivity) > 4.0. (E.g., at low and high resistivity ends of data distribution: for depth-layer D1.0 rejects 0.01% and 0.0% of data and for D29.9 rejects 0.0% and 0.05% of data).
Interpolate models across short data gaps produced by data rejection, on a line-by-line basis, for each depth layer.	*Geosoft*	Akima interpolation, across maximum number of 2 adjacent missing data (i.e., across maximum 18 m gap).
3. Model microlevelling		
Grid all depth channels (layers).	*Geosoft*	Inverse Distance Weighted (IDW) algorithm, 50 x 50 m grid cell size.
Compute microlevelling-error grids, for each depth layer.	*Geosoft*	Butterworth high-pass filter (cut-off wavelength, λ, depth dependent: D1.0: λ = 2,000 m, D3.1: λ = 1,800 m, D5.2: λ = 1,600 m, D7.5: λ = 1,400 m, D9.8 - D103.4: λ = 1,200 m) and Directional Cosine pass filter (azimuth 345°).
Resample microlevelling-error grids back to database and subtract from each depth layer.	*Geosoft*	
Convert $\log_{10}$(resistivity) values to resistivity values.	*Geosoft*	Model data simultaneously cut in proximity to the coastline.
Final gridding of microlevelled depth layers.	*Geosoft*	Inverse Distance Weighted (IDW) algorithm, 50 x 50 m grid cell size.

QC Parameter Threshold Rejection

The use of three different QC parameters was found both necessary and adequate to reliably remove poor or noisy model solutions from the dataset:

i. **"*Nsens*": normalised model sensitivity.** Absolute sensitivities (data channels SensD1.0 – SensD169.8 in Table 5.1) were normalised (divided) by a factor equal to the average sensitivity of the shallowest depth layer in the model (i.e., the average of SensD1.0), computed for the whole A6 Block. Normalised

sensitivity data channels are then available for all depth layers (NsensD1.0 – NsensD169.8). While absolute sensitivity could equally have been used for poor-model-solution rejection purposes, normalisation was performed with the aim of removing the effect on sensitivity of inversion specific parameters (e.g., data errors applied, EM data components active in the inversion, and number and thickness of model layers) – so as to derive more "universally" applicable sensitivity and threshold values, for application to other model datasets derived using different inversion parameters, including inversions of further Tellus data blocks. Whether normalised sensitivity thresholds prove to be universally applicable remains to be assessed, as further inversions on Tellus survey blocks are carried out in the future. One potential shortcoming in the strategy is, however, immediately apparent. As sensitivity is also dependent on the resistivity of the models, surveys across different geological terrains will encounter different shallow, overburden material, with different resistivity characteristics – i.e., the parameter used for normalisation – near-surface sensitivity – will not remain constant across large areas and different survey blocks.

It should be noted that the normalisation factor used here in Section 5 (and also in Section 4) is not the same as that used in the *aempy* model cross-sections presented in Section 3, where the normalisation factor is the maximum sensitivity for the whole of each model profile.

Application of the normalised sensitivity (*Nsens*) criterion is achieved in *Geosoft* using a conditional statement, where model solutions are rejected (nulled or dummied) where *Nsens* for that model solution is less than the specified threshold. Depth-dependent thresholds were defined to account for shallower layers naturally having greater sensitivities than deeper layers, with higher thresholds applied to shallower layers, and varying between 0.5 – 0.00015 (Table 5.2). As resistive model layers are intrinsically associated with low sensitivities (see discussions above in previous sections), **sensitivity threshold rejection was applied only for flight clearances greater than 90 m**, in order to avoid the unnecessary rejection, at lower flight clearances, of resistive solutions in otherwise well resolved and constrained parts of the model.

ii. **"*QCpdiff*": model percentage difference.** *QCpdiff*, as discussed previously, is the percentage difference between the forward and reverse line direction inversion models, with respect to the average model. *QCpdiff* data channels are available for all depth layers (QCpdiffD1.0 – QCpdiffD169.8).

Application of the percentage difference (*QCpdiff*) criterion is achieved in *Geosoft* using a conditional statement, where model solutions are rejected (nulled or dummied) where *QCpdiff* for that model solution is greater than 5% or less than -5% (Table 5.2).

iii. **"*P12resid*": 12 kHz in-phase misfit residual.** The misfit residual for the in-phase 12 kHz data component is calculated as the predicted model response (P12calc in Table 5.1) minus the observed response (P12npca3). The 12 kHz in-phase misfit residual was preferred, in comparison with other component's residuals, as a model-solution rejection criterion as it has low means for both the residuals and the absolute value residuals (Table 4.3), the former indicating a good fit for this component to the baseline of the observed data and the latter indicating generally good levels of fit to the observations. Lower cultural noise levels and stronger geological signal amplitudes for this component make it preferable to the 0.9 kHz in-phase and quadrature residuals.

Application of the in-phase 12 kHz residual (*P12resid*) criterion is achieved in *Geosoft* using a conditional statement, where model solutions are rejected (nulled or dummied) where *P12resid* for that model solution is greater than 108.6 ppm or less than -131.4 ppm (Table 5.2). The asymmetry of the thresholds accounts for the mean of the in-phase 12 kHz residuals being offset from the observed data baseline by -11.4 ppm (Table 4.3).

The effect of high flight clearances on the EM responses and on the inversion model solutions is clearly visible when examining these data along flight lines (Figures 5.1 and 5.2). There is a sharp and recognisable lateral transition from EM responses containing meaningful geological signal, corresponding with laterally coherent inversion solutions, to very low amplitude EM signals with low to zero geological signal, corresponding with erratic and spurious model solutions. In the example of line L6409 in Figures 5.1 and 5.2, the transition occurs at a flight clearance of around 124.3 m, for all model depth

solutions shown (1.0 m, 14.9 m and 29.9 m depth). It is not always the case that all depth layers lose coherency at the same flight clearance – in cases, shallower depth layers (or more conductive bodies) retain coherency to higher clearances than deeper layers (or more resistive bodies).

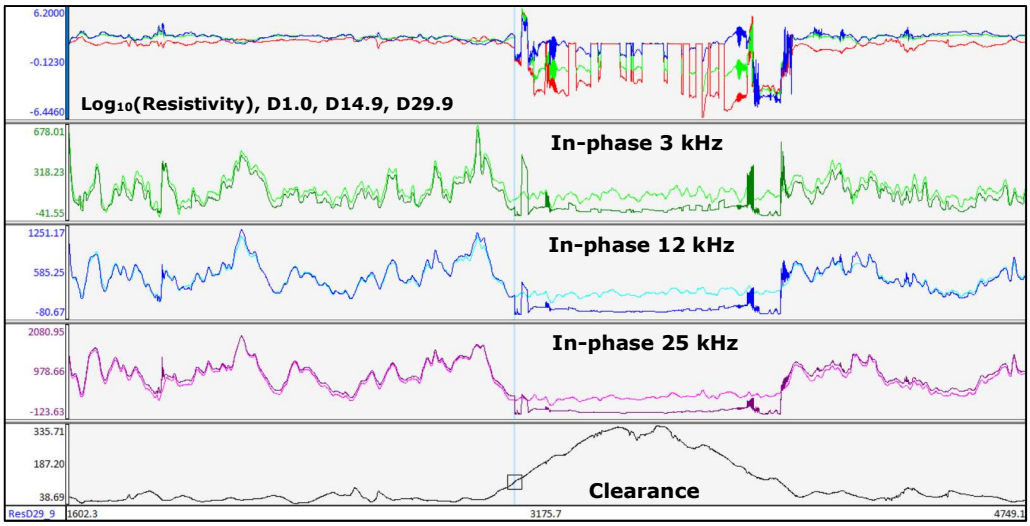

Figure 5.1: A6 Block inversion models and data fit, portion of line L6409 (18.7 km section length). (Top) Resistivity profiles for model depth-layers D1.0 (red), D14.9 (green) and D29.9 (blue). (Second from top) In-phase 3 kHz observed (light green) and predicted (dark green) responses. (Middle) In-phase 12 kHz observed (light blue) and predicted (dark blue) responses. (Second from bottom) In-phase 25 kHz observed (light violet) and predicted (dark violet) responses. (Bottom) Flight clearance (black). Cursor locality shows transition from good to poor model solutions, corresponding with flight clearance = 124.3 m. NNW is on right hand side of profile. High-fly area is located over town of Fermoy, Co. Cork.

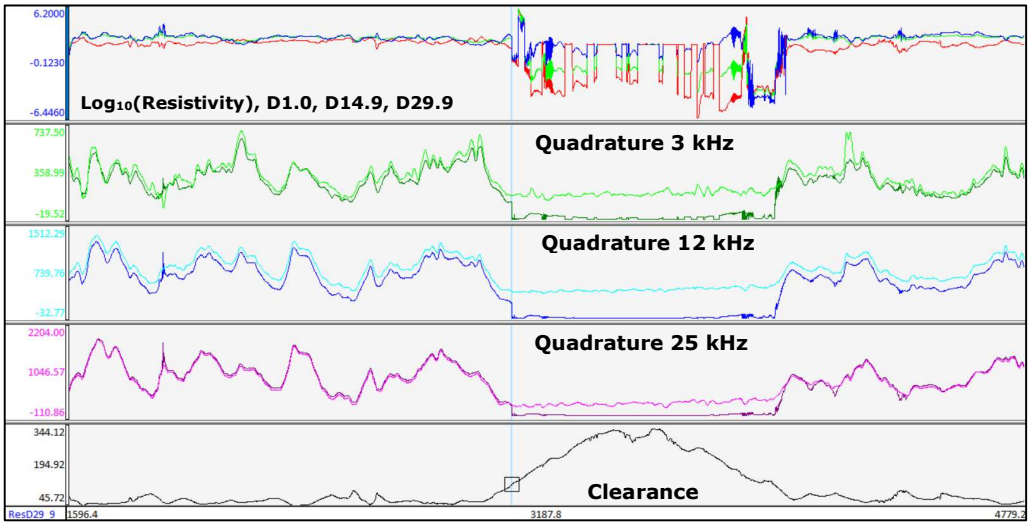

Figure 5.2: A6 Block inversion models and data fit, portion of line L6409 (18.7 km section length). (Top) Resistivity profiles for model depth-layers D1.0 (red), D14.9 (green) and D29.9

(blue). (Second from top) Quadrature 3 kHz observed (light green) and predicted (dark green) responses. (Middle) Quadrature 12 kHz observed (light blue) and predicted (dark blue) responses. (Second from bottom) Quadrature 25 kHz observed (light violet) and predicted (dark violet) responses. (Bottom) Flight clearance (black). Cursor locality shows transition from good to poor model solutions, corresponding with flight clearance = 124.3 m. NNW is on right hand side of profile. High-fly area is located over town of Fermoy, Co. Cork.

The clear, visual expression of poor model solutions, when viewed as along-line resistivity profiles (*cf.*, Figures 5.1 and 5.2), allowed appropriate threshold values for the three QC criteria to be determined empirically – through careful testing and visual assessment of a large number of flight lines and all depth layers – leading to the threshold values defined in Table 5.2 and applied to the full A6 model dataset using *Geosoft* scripts to automate the process.

The process of model-cleaning using thresholds defined for the three QC criteria, *Nsens*, *QCpdiff* and *P12resid*, is illustrated in Figures 5.3 and 5.4, for the case of model depth layer D9.8 along a 20.0 km-long section of line L6258. The green resistivity profile in these figures shows the original model solutions, and the red resistivity profile the cleaned (or accepted) model solutions. The failure of the model responses to match the average baseline of the observed 12 kHz quadrature responses, identified and discussed in Section 4 (misfit residuals), is apparent in Figure 5.3, where a clear offset between the observed and predicted responses is seen. Poor model solutions and poor fits to the observed data are associated with a high-fly zone in the middle of the line section. The cursor in Figure 5.4 shows the locality where normalised sensitivity (*NsensD9.8*) is below the applied threshold value of 0.005, corresponding with a flight clearance of 115.8 m. There are visibly poor solutions to the left of the cursor, where sensitivity is higher than the threshold, which have not been rejected by the sensitivity criterion. However, these poor solutions (with sensitivities greater than the sensitivity threshold) are rejected by both the *QCpdiff9.8* and *P12resid* criteria.

It is practically very difficult, within an automated model-cleaning scheme, to define widely applicable threshold values that will reject all poor model solutions under all circumstances, for all depths, flight clearances and model resistivities and the efficacy of the automated approach relies on the mutual support provided by the simultaneous use of three different criteria. The efficacy of the approach is further illustrated in the example of line L6245 (Figure 5.5), where the removal of all poor and unstable model solutions along the line is shown for the D9.8 depth layer. Removal of poor model

solutions on the northern end of the line, associated with high flight clearances over a series of narrow, deep valleys transected by the line, is particularly notable.

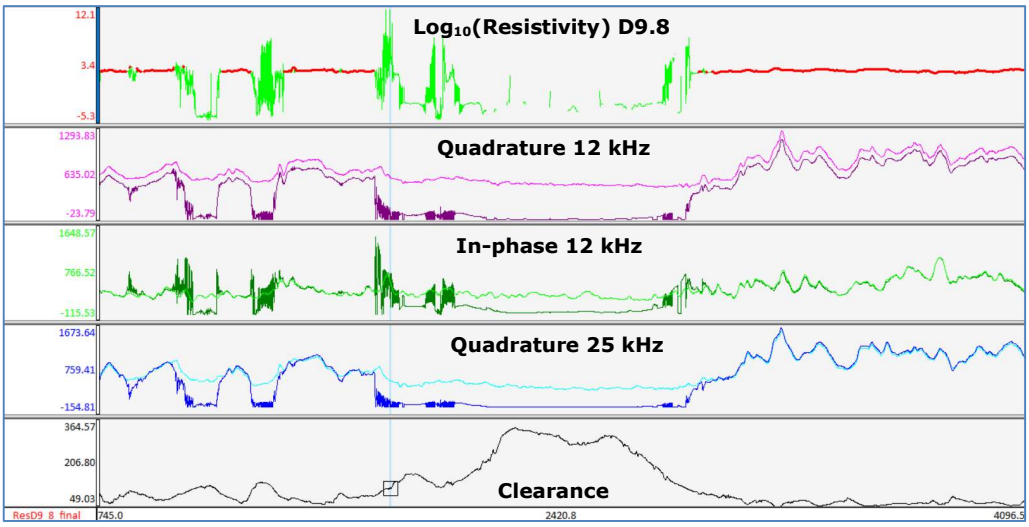

Figure 5.3: A6 Block inversion model and data fit, portion of line L6258 (20.0 km section length). (Top) Resistivity profiles for model depth layer D9.8, original and uncorrected (green) and cleaned using QC criteria (red). (Second from top) Quadrature 12 kHz observed (light violet) and predicted (dark violet) responses. (Middle) In-phase 12 kHz observed (light green) and predicted (dark green) responses. (Second from bottom) Quadrature 25 kHz observed (light blue) and predicted (dark blue) responses. (Bottom) Flight clearance (black). Cursor locality corresponding with flight clearance = 115.8 m. SSE is on right hand side of profile.

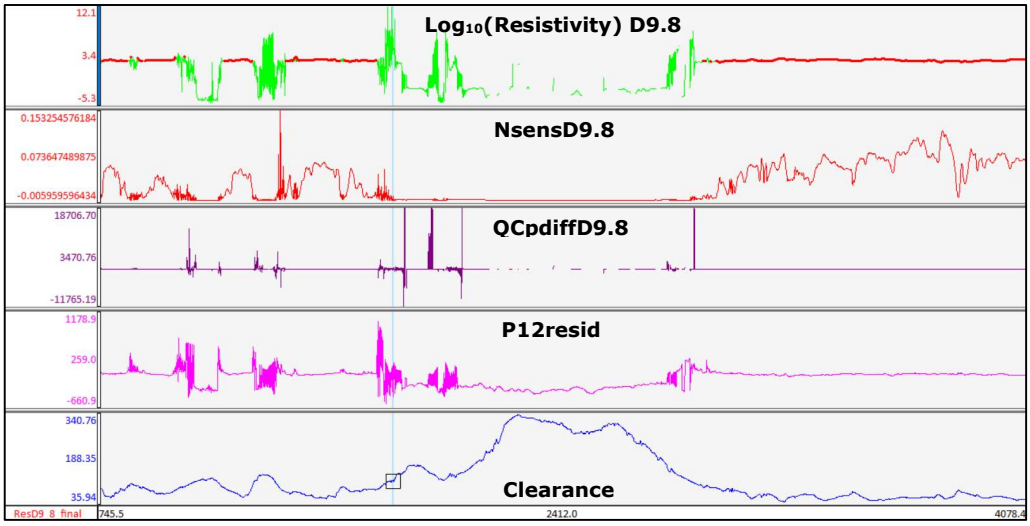

Figure 5.4: A6 Block inversion model and QC criteria, portion of line L6258 (20.0 km section length). (Top) Resistivity profiles for model depth layer D9.8, original and uncorrected (green) and cleaned using QC criteria (red). (Second from top) Normalised sensitivity – NsensD9.8 QC parameter (red). (Middle) Model percentage difference – QCpdiffD9.8 QC parameter (dark purple). (Second from bottom) In-phase 12 kHz residual – P12resid QC parameter (violet).

(Bottom) Flight clearance (blue). Cursor shows locality where NsensD9.8 value (0.000120) is less than the QC threshold = 0.005, corresponding with flight clearance = 115.8 m. SSE is on right hand side of profile.

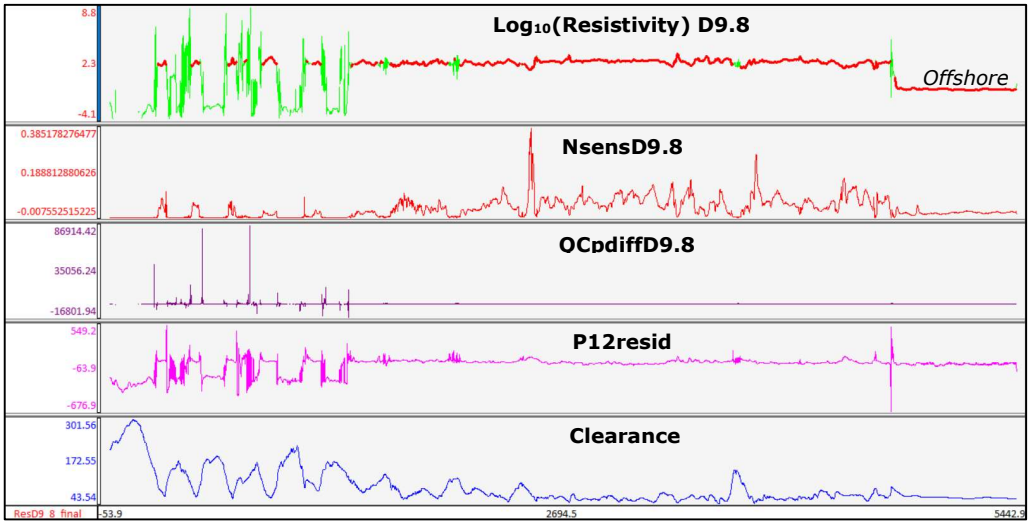

Figure 5.5: A6 Block inversion model and QC criteria, line L6245 (36.3 km line length). (Top) Resistivity profiles for model depth layer D9.8, original and uncorrected (green) and cleaned using QC criteria (red). (Second from top) Normalised sensitivity – NsensD9.8 QC parameter (red). (Middle) Model percentage difference – QCpdiffD9.8 QC parameter (dark purple). (Second from bottom) In-phase 12 kHz residual – P12resid QC parameter (violet). (Bottom) Flight clearance (blue). SSE is on right hand side of profile.

Smoothing, Outlier Resistivity Value Rejection and Interpolation

Away from high-fly areas and sources of cultural noise, resistivity values within each model depth layer generally show good lateral continuity and smooth variation from site to site (an outcome reinforced by the non-independent inversion strategy used). However, there are instances of low amplitude, site-to-site resistivity variations, where the inversion models appear to oscillate between moderately different preferred solutions from site to site. An example of the oscillating behaviour in the 9.8 m depth layer is shown in Figure 5.6, along a short 0.7 km-long section of line L6465. Poor model solutions are rejected by the three QC criteria in the central portion of the displayed section. In this example, resistivity oscillations on the flanks of the area of rejected model solutions are seen to vary between 130 - 700 Ω.m. Although these oscillations are reflected in all three QC criteria, *NsensD9.8*, *QCpdiffD9.8* and *P12resid*, the model solutions are not rejected as the QC thresholds are not exceeded. Application of a 10-

fiducial (~60 m wavelength) low-pass filter, on a line-by-line basis, was found to effectively remove such site-to-site resistivity oscillations (see Figure 5.6), as well as isolated model spikes not caught by the QC rejection criteria, without altering the resistivity solutions away from problematic areas. **The 10-fiducial low-pass filter was applied to all depth layers in the dataset.**

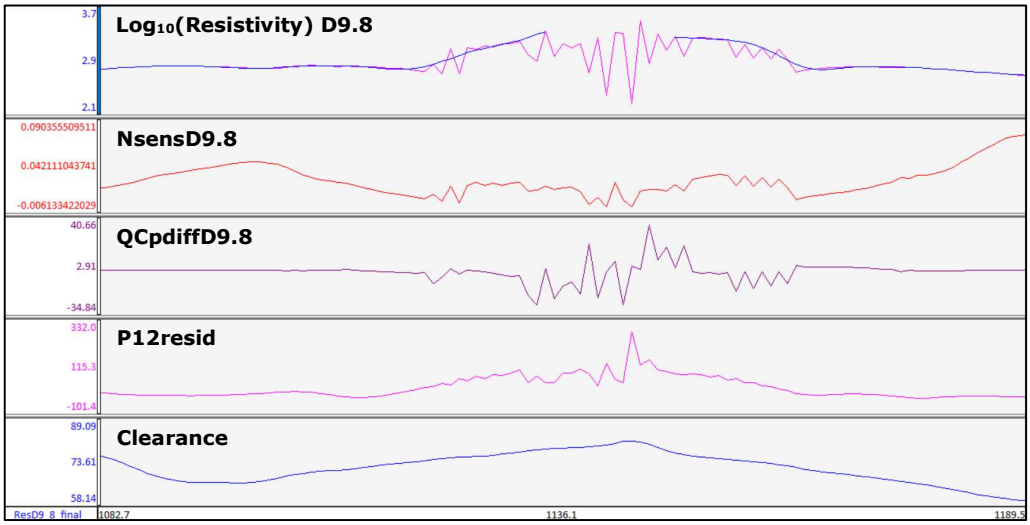

Figure 5.6: A6 Block inversion model and QC criteria, portion of line L6465 (0.7 km-long line section). (Top) Resistivity profiles for model depth layer D9.8, original and uncorrected (violet) and low-pass filtered (10-fiducial) (blue). (Second from top) Normalised sensitivity – NsensD9.8 QC parameter (red). (Middle) Model percentage difference – QCpdiffD9.8 QC parameter (dark purple). (Second from bottom) In-phase 12 kHz residual – P12resid QC parameter (violet). (Bottom) Flight clearance (blue).

In a small number of instances, extremely low or high resistivity values are returned in the inversion model solutions, and these extreme values are not always captured and rejected by the QC criteria. **Extreme values have therefore been rejected using the following criteria: reject solutions where log10(resistivity) < -1.0 (= 0.1 Ω.m) or log10(resistivity) > 4.0 (= 10,000 Ω.m).** At the low and high resistivity ends of the data distribution, these resistivity limits reject, for example, 0.01% and 0.0% of the model data for the D1.0 depth-layer and 0.0% and 0.05% of the data for the D29.9 layer.

The final model-cleaning process applied is that of interpolation, to fill in short gaps in the along-flight-line resistivity profiles resulting from very localised rejection of poor model solutions (e.g., spikes). **An Akima interpolation was applied on a line-by-line**

basis, for all depth layers, across a maximum number of 2 adjacent missing data points (i.e., across a maximum gap of 18 m). The size of the gap filled by the interpolation is commensurate with the size of the EM imaging footprint on the ground and in the subsurface.

Gridded examples, for a number of representative depth layers (3.1 m, 12.3 m, 29.9 m and 62.6 m depths) taken from the final cleaned resistivity dataset, are provided in the section below.

Microlevelling of Resistivity Model Data

Although the EM response data used as input for the resistivity inversions are well levelled (but not microlevelled), minor residual line-to-line variations in these data manifest themselves, amplified, as line-to-line variations in the resistivities of the inversion models. Line-to-line variations (or levelling errors) are more pronounced in the shallower model layers above 10 m depth (e.g., Figure 5.6, showing resistivity grids for the 3.1 m depth layer). Microlevelling of the final, cleaned model dataset was carried out to remove line-to-line variations, treating each depth layer separately and following the workflow summarised in Table 5.2 and described in further detail below. The resistivity data for twenty-seven depth layers, from D1.0 to D103.4, were microlevelled. Examples of resistivity data grids, pre- and post-microlevelling, are shown in Figures 5.7, 5.9, 5.10 and 5.11 for depth layers D3.1, D12.3, D29.9 and D62.6 respectively.

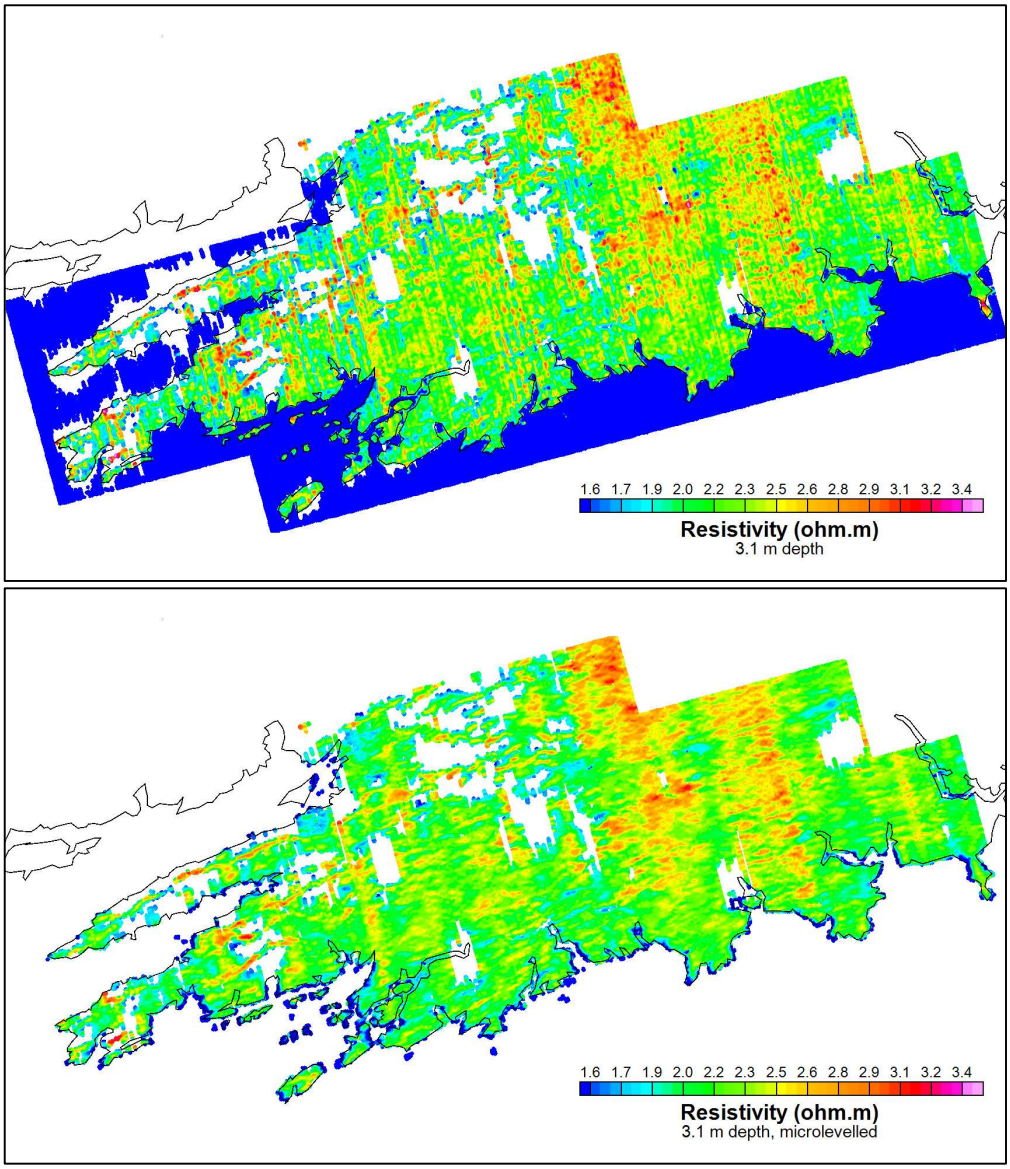

Figure 5.7: A6 Block EM inversion – grid maps of resistivity for 3.1 m depth-layer. (Top) Final cleaned dataset. (Bottom) Final cleaned dataset after microlevelling. Models are blanked where solutions fall outside the threshold limits of the three QC criteria applied: NsensD3.1, QCpdiffD3.1 and P12resid. Microlevelled data are further blanked in proximity of the coastline. Inverse Distance Weighted gridding is used, with 50 x 50 m grid mesh. Colour scale used: log-linear distribution, with conductors shown in blue and resistors in red. Irish coastline shown (black line).

Following gridding of the final, clean resistivities for all depth layers, the microlevelling procedure consists of computing microlevelling-error grids, in which line-to-line differences (errors) are isolated, by applying dual Butterworth high-pass and Directional Cosine filters to the final resistivity grids. The example microlevelling-error grid of Figure

5.8, for depth layer D3.1, illustrates the line-to-line differences extracted from the final D3.1 resistivity grid of Figure 5.7 (upper grid). Subtraction of the microlevelling-errors yields the final microlevelled D3.1 resistivity grid of Figure 5.7 (lower grid). Practically, the subtraction of microlevelling-errors is achieved by re-sampling the microlevelling-error grids back to the line database, as a new data channel, where they are subtracted from the resistivity data channels, to produce line-based, microlevelled resistivity data for each depth layer – the final product of the EM inversions. It is noted that microlevelling was carried out with resistivities in the $\log_{10}$ domain. Log_{10}(resistivity) values are converted to resistivity values for the public release of the inversion models.

Depth-dependence was required in the specification of the cut-off wavelength of the Butterworth high-pass filter that was applied to isolate levelling errors from the resistivity model data (see specifications in Table 5.2). At shallower depths (D1.0 – D7.5), the resistivity data grids (pre-microlevelling) are characterised by longer wavelength levelling errors (in a direction perpendicular to the line direction), requiring longer cut-off wavelengths in the filter. Compared with the 1,200 m cut-off wavelength for depth layers D9.8 and greater, cut-off wavelengths used increased from 1,400 m for D7.5 to 2,000 m for D1.0 at intervals of 200 m.

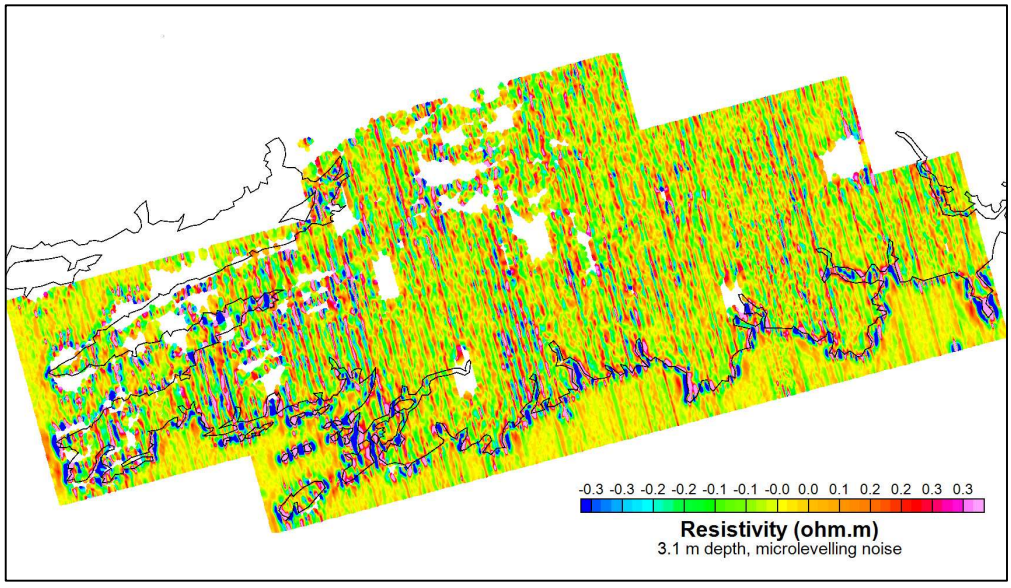

Figure 5.8: A6 Block EM inversion – grid map of microlevelling-error for 3.1 m depth-layer. Data are blanked where original resistivity model solutions fall outside the threshold limits of the three QC criteria applied: NsensD3.1, QCpdiffD3.1 and P12resid. Inverse Distance Weighted

gridding is used, with 50 x 50 m grid mesh. Colour scale used: log-linear distribution. Irish coastline shown (black line).

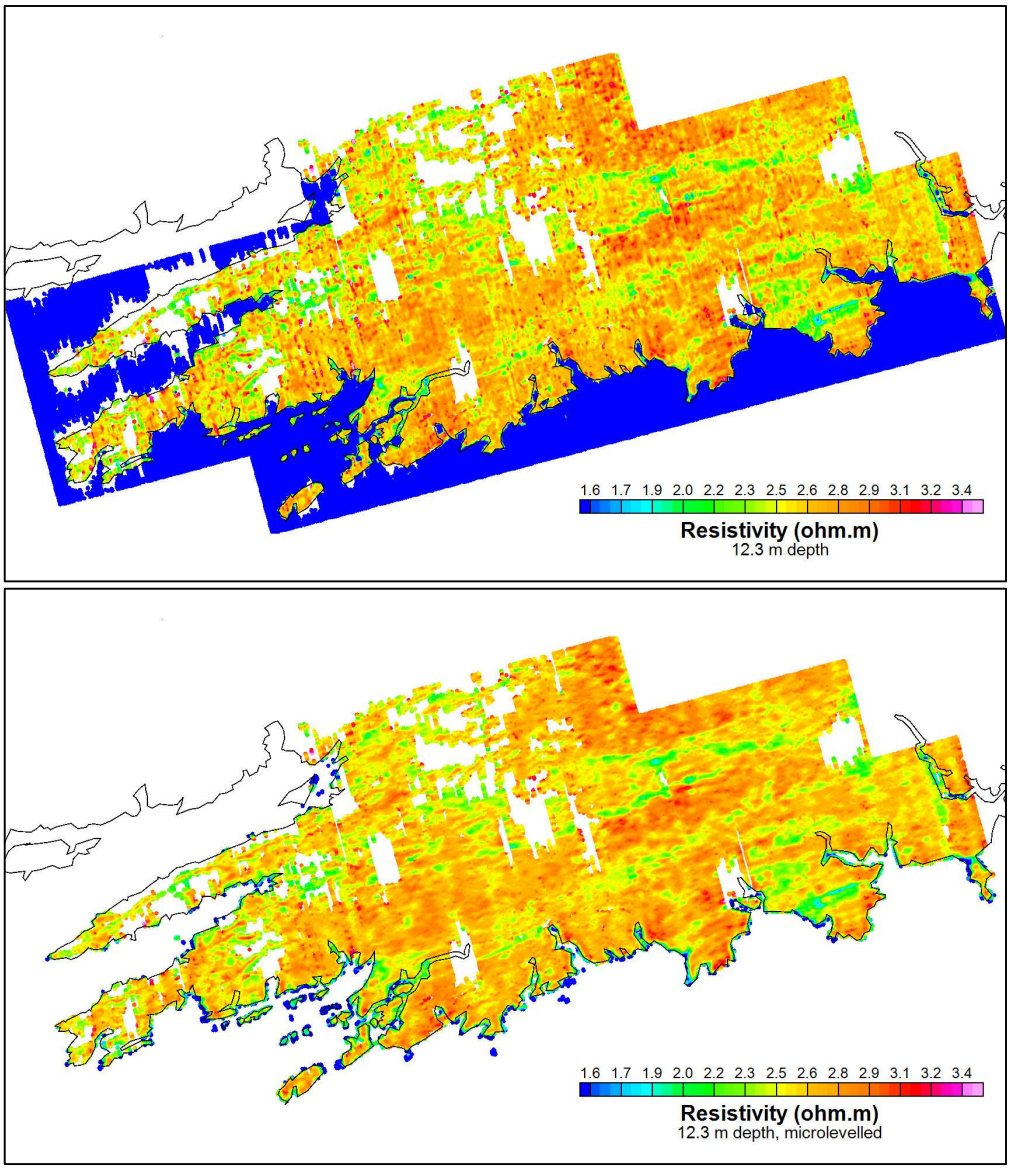

Figure 5.9: A6 Block EM inversion – grid maps of resistivity for 12.3 m depth-layer. (Top) Final cleaned dataset. (Bottom) Final cleaned dataset after microlevelling. Models are blanked where solutions fall outside the threshold limits of the three QC criteria applied: NsensD12.3, QCpdiffD12.3 and P12resid. Microlevelled data are further blanked in proximity of the coastline. Inverse Distance Weighted gridding is used, with 50 x 50 m grid mesh. Colour scale used: log-linear distribution, with conductors shown in blue and resistors in red. Irish coastline shown (black line).

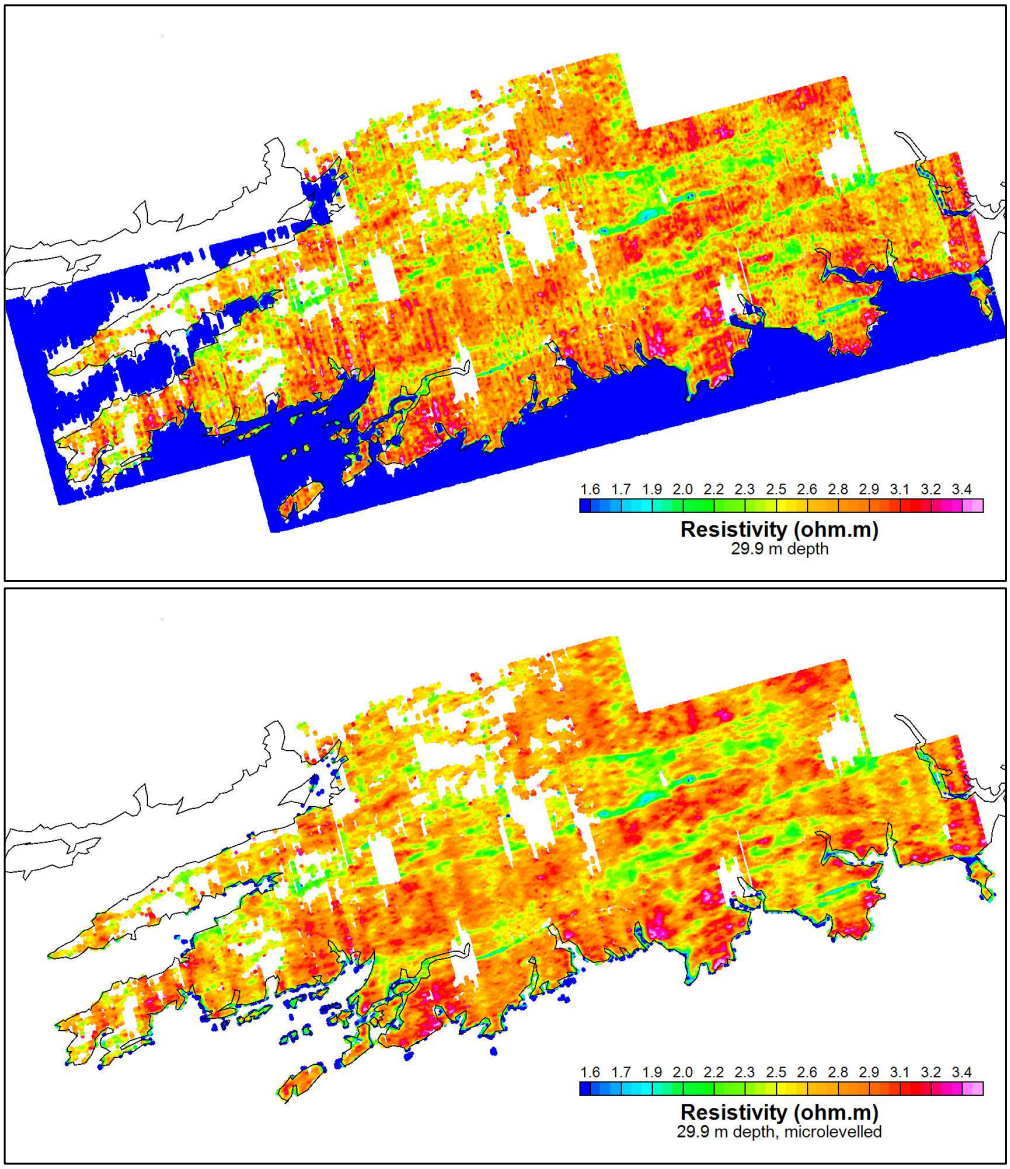

Figure 5.10: A6 Block EM inversion – grid maps of resistivity for 29.9 m depth-layer. (Top) Final cleaned dataset. (Bottom) Final cleaned dataset after microlevelling. Models are blanked where solutions fall outside the threshold limits of the three QC criteria applied: NsensD29.9, QCpdiffD29.9 and P12resid. Microlevelled data are further blanked in proximity of the coastline. Inverse Distance Weighted gridding is used, with 50 x 50 m grid mesh. Colour scale used: log-linear distribution, with conductors shown in blue and resistors in red. Irish coastline shown (black line).

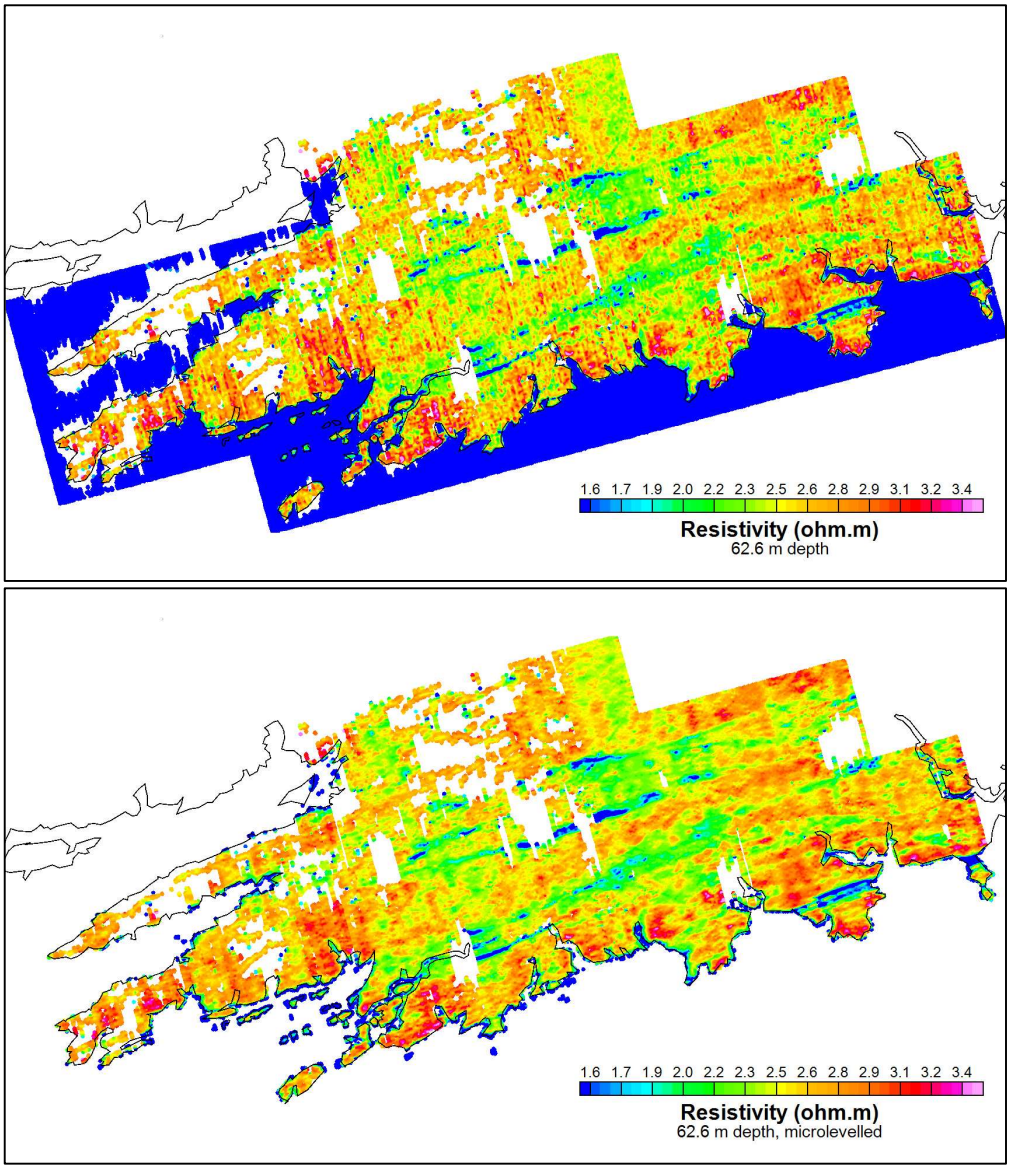

Figure 5.11: A6 Block EM inversion – grid maps of resistivity for 62.6 m depth-layer. (Top) Final cleaned dataset. (Bottom) Final cleaned dataset after microlevelling. Models are blanked where solutions fall outside the threshold limits of the three QC criteria applied: NsensD62.6, QCpdiffD62.6 and P12resid. Microlevelled data are further blanked in proximity of the coastline. Inverse Distance Weighted gridding is used, with 50 x 50 m grid mesh. Colour scale used: log-linear distribution, with conductors shown in blue and resistors in red. Irish coastline shown (black line).

Model Data Released

Bulk examination of inversion sensitivity profiles across the A6 Block indicate a general, marked reduction in model sensitivities below depths of around 50 – 60 m for model

resistivities in the broad range 100 – 800 Ω.m (roughly ±1σ or 68% of the data for layer D62.6). Below around 60 m depth, the resistivity models show little variation with increasing depth, suggesting they are largely weakly constrained extrapolations of well-constrained resistivity values modelled at shallower depth. Models for public release therefore do not include layers deeper than 62.6 m, providing a dataset with a reliable maximum depth of investigation. The offshore model solutions have additionally been blanked for data release.

EM inversion resistivity models, to a depth of 62.6 m, are released in a number of different data formats. The first dataset below constitutes the final and complete EM model dataset, with other datasets released being derivative products of this "master" dataset.

i. **Ascii, flight-line and site ordered dataset.** Complete, full-resolution dataset with nominal 6 m spacing between model sites. Resistivity data for twenty depth-layers, from 1.0 m to 62.6 m depth, are provided as separate channels (columns) in the dataset. The data are suitable for manipulation to produce either section or map views of the models. Surface topography (DEM) with respect to sea-level is included for each site, allowing models to be plotted beneath a topographic reference in section view.

   File name: [A6_EM_INV_MODELS_OHMM.XYZ].

   File format: *Geosoft* [.XYZ]. Suitable for import into to any software with ascii import capability.

   Dataset description: Appendix 1.

ii. **Resistivity grids on 50 x 50 m mesh.** Provided separately for twenty depth-layers, from 1.0 m to 62.6 m depth.

   File formats: *Geosoft* grid [.GRD] and georeferenced tiff [.TIF]

   Dataset description: Appendix 2.

6. Conclusions

The A5 Block (GSI, 2020a) was used as the first test case to develop a new workflow for 1-D inversion modelling of Tellus EM data, built around the capacities provided by the new, *Python* based software toolbox, *aempy*. Inversion of the WFD (Waterford) Block followed A5 (GSI, 2020b). The A6 Block reported on here, has utilised the same inversion workflow as the previous two blocks. Testing of various aspects of the workflow on the A6 dataset, including the application of the Principal Component Analysis noise-rejection filter and the use of non-independent inversion modelling within the forward-reverse-average (FRA) modelling strategy, confirmed the workflow to be robust and suitable for the A6 dataset. Inversion regularisation parameter ($\tau 0$ and $\tau 1$) tests identified parameter values best suited for the inversion of the A6 dataset.

Parameters utilised for the A6 Block that represent (modest) departures from those previously used include: the use of a 5-fiducial (rather than 20-fiducial) low-pass filter applied to the laser-altimeter clearance data prior to inversion, and the use of a $\tau 1$ regularisation parameter value of 2.9 (rather than $\tau 1 = 6.0$). While depth-dependent model sensitivity thresholds specific to the characteristics of the A6 model dataset were required, the value of the availability and use of three different model QC criteria (sensitivity, model percentage difference and misfit residuals) in the model-cleaning component of the workflow was reconfirmed.

1-D resistivity models were computed for a total of 2,145,192 sites on 465 flight-lines using Tikhonov-type, regularised inversion, implemented in *aempy*. The inversions produced a good overall quality of fit with respect to the observed EM responses: a mean RMS error of 1.388 and mean absolute value misfit residual of 60.6 ppm, calculated for sites with flight-clearance < 120 m (1,796,925 sites, or 83.8% of the A6 total). The RMS error reported is normalised by the data errors applied (60.0 ppm for all eight EM data components), with an RMS error value of 1.0 indicating a model fit to within the data error. Misfit residual is defined as the predicted model response minus the observed response, separately for each component (from which the mean value is derived).

Assessment of the model misfit residuals also provides insights into several broader characteristics of the A6 Block dataset, with potential to support the on-going EM data processing work of Tellus contractor SGL. The largest misfit residuals were recorded for the quadrature component at 12 kHz (-98.7 ppm average misfit, predicted response lower in amplitude than observed response), with the implication that the inversion models were unable to match the baseline of the observed 12 kHz quadrature responses while simultaneously matching the baselines of the other data components. In the case of the A5 Block, a simultaneous match of the observed baselines for the 12 kHz and 25 kHz in-phase components was problematic, while for the WFD Block it was the matching of the 12 kHz and 25 kHz quadrature component baselines that was problematic. As each of the component data baselines are retrospectively updated for consistency across all survey bocks by contractor SGL on completion of each new Tellus block, there may be scope for using the average misfit residual statistics from each completed inversion block as an additional constraint on the work.

Model cleaning – rejection of poor model solutions arising in high-fly and high-cultural-noise survey areas – was carried out in *Geosoft Oasis Montaj* software, using scripts that automated the sequential steps in the cleaning process. Three different QC parameters were confirmed to be both necessary and adequate for rejection of poor solutions: (i) *Nsens*, the normalised model sensitivity, applied only where flight-clearance > 90 m (ii) *QCpdiff*, the percentage difference between the forward and reverse line direction inversion models, with respect to the average model, and (iii) *P12resid*, the 12 kHz in-phase misfit residual. Rejection threshold values for the three QC parameters were determined empirically by closely examining the relationship between the model solutions (good and bad) and the QC parameters, at all depths in the model and on multiple flight-lines across the survey area. The initial 35 layers of the inversion were truncated to 20 layers, from surface to 62.6 m depth, taking into account the marked reduction in model sensitivity below around 50 – 60 m depth observed broadly across the survey area. The final model dataset, therefore, retains only model solutions that pass the screening of the QC criteria and fall within a depth range where the EM data provide a strong model constraint.

The ~60 m depth of investigation and the lateral and vertical resolution characteristics of the model dataset make it well suited to a range of different possible applications where knowledge of shallow subsurface geology is required. Examples of potential uses

include, but are not limited to: bedrock mapping beneath overburden and high-resolution mapping of shallow geological strata; identification and mapping of shallow sand and gravel bodies; mapping of quaternary sedimentary deposits; soil mapping; thickness mapping of peat bogs; and shallow aquifer mapping.

7. References

Golub, G. and van Loan, C.F., 1996. *Matrix Computations*. The Johns Hopkins University Press, Baltimore, Maryland, 3rd Edition, pp. 694.

GSI, 2020a. *Tellus A5 Block: aempy Electromagnetic Inversion Report*. Unpublished Technical Report, Geological Survey Ireland, February, 2020.

GSI, 2020b. *Tellus Waterford (WFD) Block: aempy Electromagnetic Inversion Report*. Unpublished Technical Report, Geological Survey Ireland, July, 2020.

Kiyan, D. and Rath, V., 2017. *Inverse Methods for Airborne Electromagnetic Data from the Tellus Surveys: The aempy Toolbox*. Unpublished Report and User Manual, Dublin Institute for Advanced Studies, Ireland, March 21, 2017.

Kiyan, D., Rath, V., Delhaye, R., Ture, M.D. and Hodgson J., 2017. Imaging the Earth's Near Surface Using the Tellus Airborne Electromagnetic Data. Unpublished Presentation, Tellus Stakeholder Day, Geological Survey Ireland, Dublin, November 6, 2017.

Kiyan, D., Rath, V., Muller, M.R., Ture, M.D. and Hodgson, J., in review. 1-D Inversion of Frequency-Domain Airborne Electromagnetic Data using the *aempy* Toolbox. Manuscript submitted and in review.

Lanczos, C., 1961. *Linear Differential Operators*. D. Van Nostrand Co. Ltd, London, pp. 576.

Minsley, B.J., Smith, B.D., Hammack, R., Sams, J.I. and G. Veloski, G., 2012. Calibration and filtering strategies for frequency domain electromagnetic data. *Journal of Applied Geophysics*, **80**, 56–66.

Reninger, P.-A., Martelet, G., Deparis, J., Perrin, J. and Y. Chen, Y., 2011. Singular value decomposition as a denoising tool for airborne time domain electromagnetic data. *Journal of Applied Geophysics*, **75(2)**, 264 – 276.

Sengpiel, K. P., 1988. Approximate Inversion of Airborne EM Data from a Multilayered Ground. *Geophysical Prospecting*, **36**, 446-459.

Sengpiel, K.-P. and Siemon, B., 1998. Examples of 1D Inversion of Multifrequency AEM Data from 3D Resistivity Distributions. *Exploration Geophysics*, **29**, 133-141.

SGL, 2019. *Fixed-Wing High-Resolution Aeromagnetic, Gamma-ray Spectrometric and Frequency-Domain Electromagnetic Survey, Tellus A5 Block, Republic of Ireland, 2019*. Unpublished Technical Report, Sander Geophysics Limited, Canada, August, 2019.

Appendix 1: A6_EM_INV_MODELS_OHMM_ReadMe.txt

==========

This readme file relates to data from file: A6_EM_INV_MODELS_OHMM.XYZ (for lines L6001 - L6465)

1-D inversion model data derived from airborne electromagnetic (EM) geophysical data collected between August 2018 and June 2019.
by Geological Survey Ireland, Tellus Project.

Notepad text editor is recommended to read the data file correctly.

Data type: The data are 1-D EM inversion models for the A6 survey block.
Data modelling: Inversion models computed using aempy software, Tikhonov-type 1-D layered model inversion.
Model solutions nulled where failing QC criteria. Microlevelled.
Date of collection: EM data collected between 25/08/2018 and 15/06/2019.
Geographical extent: The A6 Survey block covers the majority of County Cork, Ireland.
Contractor: Sander Geophysics Ltd
Client: Geological Survey Ireland (GSI)
Date of data release: 16 July 2020

For data queries please contact: tellus@gsi.ie

The data file contains the channels (columns) described below.
File header lines at start of file specified with "/" or "//" characters (without inverted commas)
The dataset is flight-line ordered, with a line separator "LINE line_number" at the start of each flight-line in the file
(without inverted commas and where line_number is numeric, e.g., 6001).

==========

File Name: A6_EM_INV_MODELS_OHMM.XYZ

Name	Units	Description
LINE	-	Line Number
ITM_X	m	X coordinate, IRENET95 ITM
ITM_Y	m	Y coordinate, IRENET95 ITM
DEM	m	Digital Elevation Model with respect to Mean Sea Level, from Laser Altimeter and GPS Z data
ALT	m	Flight clearance above Terrain, from Laser Altimeter
ResD1_0_ohmm	ohm.m	Model resistivity at 1.0 m depth, data nulled where failing QC criteria
ResD3_1_ohmm	ohm.m	Model resistivity at 3.1 m depth, data nulled where failing QC criteria
ResD5_2_ohmm	ohm.m	Model resistivity at 5.2 m depth, data nulled where failing QC criteria
ResD7_5_ohmm	ohm.m	Model resistivity at 7.5 m depth, data nulled where failing QC criteria
ResD9_8_ohmm	ohm.m	Model resistivity at 9.8 m depth, data nulled where failing QC criteria
ResD12_3_ohmm	ohm.m	Model resistivity at 12.3 m depth, data nulled where failing QC criteria
ResD14_9_ohmm	ohm.m	Model resistivity at 14.9 m depth, data nulled where failing QC criteria
ResD17_6_ohmm	ohm.m	Model resistivity at 17.6 m depth, data nulled where failing QC criteria
ResD20_5_ohmm	ohm.m	Model resistivity at 20.5 m depth, data nulled where failing QC criteria
ResD23_5_ohmm	ohm.m	Model resistivity at 23.5 m depth, data nulled where failing QC criteria
ResD26_6_ohmm	ohm.m	Model resistivity at 26.6 m depth, data nulled where failing QC criteria
ResD29_9_ohmm	ohm.m	Model resistivity at 29.9 m depth, data nulled where failing QC criteria
ResD33_3_ohmm	ohm.m	Model resistivity at 33.3 m depth, data nulled where failing QC criteria
ResD36_9_ohmm	ohm.m	Model resistivity at 36.9 m depth, data nulled where failing QC criteria
ResD40_7_ohmm	ohm.m	Model resistivity at 40.7 m depth, data nulled where failing QC criteria
ResD44_7_ohmm	ohm.m	Model resistivity at 44.7 m depth, data nulled where failing QC criteria
ResD48_9_ohmm	ohm.m	Model resistivity at 48.9 m depth, data nulled where failing QC criteria
ResD53_2_ohmm	ohm.m	Model resistivity at 53.2 m depth, data nulled where failing QC criteria
ResD57_8_ohmm	ohm.m	Model resistivity at 57.8 m depth, data nulled where failing QC criteria
ResD62_6_ohmm	ohm.m	Model resistivity at 62.6 m depth, data nulled where failing QC criteria

==========

Appendix 2: A6_EM_INV_MODELS_OHMM_GRIDS_ReadMe.txt

==========

This readme file relates to raster grids provided in the file: [A6_EM_INV_MODELS_OHMM_GRIDS.zip]

Raster grids of 1-D inversion model data derived from airborne electromagnetic (EM) geophysical data collected between August 2018 and June 2019.
by Geological Survey Ireland, Tellus Project.

Data type: Data are raster grids of 1-D EM inversion models for the A6 survey block.
Data modelling: Inversion models computed using aempy software, Tikhonov-type 1-D layered model inversion. Model solutions nulled where failing QC criteria. Microlevelled. Gridded at 50 m x 50 m mesh using Inverse Distance Weighted algorithm.
Date of collection: EM data collected between 25/08/2018 and 15/06/2019.
Geographical extent: The A6 Survey block covers the majority of County Cork, Ireland.
Contractor: Sander Geophysics Ltd
Client: Geological Survey Ireland (GSI)
Date of data release: 16 July 2020

Two different georeferenced grid formats are provided for the Tellus geophysical data grids:

.grd files are Geosoft grid files and can be opened in: GIS software including Geosoft, ArcGIS (only with Geosoft ArcGIS plugin) and MAPINFO.
.tif files are georeferenced coloured raster files (GeoTiff files). Resolution 170 dpi (equivalent to 50.0 m ground units).
Colour scale for .tif images: log-linear, blue to red, from 31.62 to 3162 ohm.m - as illustrated in image file "Resistivity_colour_scale.tif"

Instructions on how to display the grids with the correct colour ramp in ArcGIS and QGIS are in the [ArcGIS_Colour_Ramp_gxf_InstructionsReadMe.pdf] and [QGIS_Colour_Ramp_gxf_InstructionsReadMe.pdf] files included in this .zip.

Images are intended to be viewed with in the Geosoft Clra 32 colour ramp. Included in this .zip file are an ArcGIS style file [Geosoft.Style] and an QGIS XML Colour ramp [Geosoft_Clra_32_qgis.XML] that contain Geosoft Clra 32 colour ramps.

For data queries please contact: tellus@gsi.ie

The delivered grids are described below:

Name	Unit	DESCRIPTION
A6_ResD1_0_ohmm_IDW	ohm.m	Model resistivity grid at 1.0 m depth, data nulled where failing QC criteria
A6_ResD3_1_ohmm_IDW	ohm.m	Model resistivity grid at 3.1 m depth, data nulled where failing QC criteria
A6_ResD5_2_ohmm_IDW	ohm.m	Model resistivity grid at 5.2 m depth, data nulled where failing QC criteria
A6_ResD7_5_ohmm_IDW	ohm.m	Model resistivity grid at 7.5 m depth, data nulled where failing QC criteria
A6_ResD9_8_ohmm_IDW	ohm.m	Model resistivity grid at 9.8 m depth, data nulled where failing QC criteria
A6_ResD12_3_ohmm_IDW	ohm.m	Model resistivity grid at 12.3 m depth, data nulled where failing QC criteria
A6_ResD14_9_ohmm_IDW	ohm.m	Model resistivity grid at 14.9 m depth, data nulled where failing QC criteria
A6_ResD17_6_ohmm_IDW	ohm.m	Model resistivity grid at 17.6 m depth, data nulled where failing QC criteria
A6_ResD20_5_ohmm_IDW	ohm.m	Model resistivity grid at 20.5 m depth, data nulled where failing QC criteria
A6_ResD23_5_ohmm_IDW	ohm.m	Model resistivity grid at 23.5 m depth, data nulled where failing QC criteria
A6_ResD26_6_ohmm_IDW	ohm.m	Model resistivity grid at 26.6 m depth, data nulled where failing QC criteria
A6_ResD29_9_ohmm_IDW	ohm.m	Model resistivity grid at 29.9 m depth, data nulled where failing QC criteria
A6_ResD33_3_ohmm_IDW	ohm.m	Model resistivity grid at 33.3 m depth, data nulled where failing QC criteria
A6_ResD36_9_ohmm_IDW	ohm.m	Model resistivity grid at 36.9 m depth, data nulled where failing QC criteria
A6_ResD40_7_ohmm_IDW	ohm.m	Model resistivity grid at 40.7 m depth, data nulled where failing QC criteria
A6_ResD44_7_ohmm_IDW	ohm.m	Model resistivity grid at 44.7 m depth, data nulled where failing QC criteria
A6_ResD48_9_ohmm_IDW	ohm.m	Model resistivity grid at 48.9 m depth, data nulled where failing QC criteria
A6_ResD53_2_ohmm_IDW	ohm.m	Model resistivity grid at 53.2 m depth, data nulled where failing QC criteria
A6_ResD57_8_ohmm_IDW	ohm.m	Model resistivity grid at 57.8 m depth, data nulled where failing QC criteria
A6_ResD62_6_ohmm_IDW	ohm.m	Model resistivity grid at 62.6 m depth, data nulled where failing QC criteria